A diffuse-interface model for structure development in flow

Document status and date:
Published: 01/01/1999

Document Version:
Publisher's PDF, also known as Version of Record (includes final page, issue and volume numbers)

Please check the document version of this publication:

• A submitted manuscript is the version of the article upon submission and before peer-review. There can be important differences between the submitted version and the official published version of record. People interested in the research are advised to contact the author for the final version of the publication, or visit the DOI to the publisher's website.
• The final author version and the galley proof are versions of the publication after peer review.
• The final published version features the final layout of the paper including the volume, issue and page numbers.

Link to publication

Download date: 23. Aug. 2022

A Diffuse-Interface Model for Structure Development in Flow

Maykel Verschueren

A Diffuse-Interface Model for Structure Development in Flow

A Diffuse-Interface Model for Structure Development in Flow

Proefschrift

door

Michael Verschueren

geboren te Nieuw-Ginneken

Dit proefschrift is goedgekeurd door de promotoren:

    prof.dr.ir. H.E.H. Meijer
    en
    prof.dr.ir. F.P.T. Baaijens

Copromotor:

    dr.ir. F.N. van de Vosse

CONTENTS

Chapter 1

INTRODUCTION

Structure development, induced by phase separation, phase inversion, interfacial deformations, coalescence or break-up, is frequently encountered in modern technology and industrial processing (Edwards *et al.*, 1991). Examples are provided by the following processes and technologies: food processing, hollow porous fibre spinning, oil recovery , ink-jet printing, paper making, coating processes, membrane technology and the production of paint and cosmetics. The quality of the industrial products and technologies mentioned can be further improved if one knows how to control and manipulate structure development. One way to obtain a better understanding of structure development is through modelling. In this thesis we are mainly concerned with finding a suitable physical model and the appropriate numerical implementation to describe structure development.

Basically, we can distinguish two ways to induce structure development: thermodynamically and mechanically. Firstly, a system which is not in thermodynamic equilibrium can separate into phases, which is obviously a form of structure development. Phase separation can be induced in several ways: for example by changing the temperature or by adding a foreign component. Secondly, an imposed flow or a pressure gradient can also affect the structure: it can result in coalescence or break-up of fluid domains or in mechanical instabilities of interfaces. In most cases mechanically and thermodynamically induced structure development can not be decoupled. In systems with a spatial dimension larger than one they are obviously coupled through interfacial tension and curvature. Other couplings occur when properties such as density, viscosity or interfacial tension depend on the composition of the system. Therefore, to be able to model structure development one has to include both non-equilibrium thermodynamics and multicomponent hydrodynamics, in a coupled way. Furthermore, processes such as phase separation, coalescence and break-up involve topological changes: interfaces can (dis)appear or intersect. An appropriate model also has to be able to describe these topological changes.

In the classical approach to multicomponent flow, an interface is assumed to be sharp (see figure 1.1) and appropriate boundary conditions are applied to connect the various components. Solving the equations of fluid dynamics therefore involves solving a moving boundary problem. The most 'natural' numerical technique in this case is the tracking method (Hyman, 1984; Unverdi and Tryggvason, 1992): the discretisation is such that grid points follow the interface. In case of topological changes, which are often encountered during structure

development, the tracking method is inconvenient, since complicated re-meshing is necessary. To overcome this problem, Brackbill *et al.* (1991) developed a continuum surface force (CSF) method in which the sharp interface is replaced by an artificial, continuous 'colour' function. This colour function is used to determine the position and the geometry of the interface. Interfacial tension can now be included in the equation of motion as a body force. A direct application of boundary conditions is no longer required in this case and a fixed grid numerical method can be used, which is convenient in case of topological changes. The disadvantage of the CSF method is that the colour function is an arbitrary function without a physical meaning. It can be shown that numerical results are sensitive to the choice of this colour function (Lowengrub and Truskinovsky, 1998).

In diffuse-interface theories, which go back to the ideas of van der Waals (1979), the interface also has a non-zero thickness, but it is no longer arbitrary. It is determined by the molecular force balance at the interface and its value ξ (see figure 1.1) is closely related to the
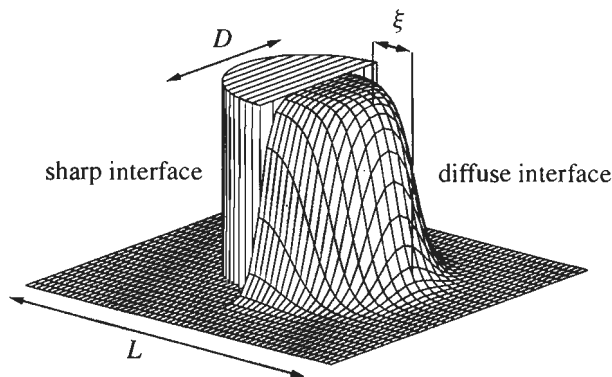
Figure 1.1: Schematic picture of a classical sharp interface and a diffuse interface.

finite range of molecular interactions (Rowlinson and Widom, 1989). Thermodynamically, the finite interaction range is represented by a non-local effect in the free energy: the local free energy density not only depends on the local composition, but also on the composition of the immediate environment (Davis and Scriven, 1982). Cahn and Hilliard (1958) used a Taylor expansion of the free energy density about the homogeneous state. In this way, the non-local effect is represented by a dependence on local composition gradients rather than non-local composition. Non-classical expressions for the chemical potential and the stress tensor can then be derived in differential form, which allows a direct coupling with the equations of fluid dynamics.

By using the diffuse-interface approach instead of the classical approach we introduce a new length scale: the interfacial thickness ξ. Typically, ξ is about 0.1 nm for small-molecule systems and can go up to 1 nm for polymer systems. The domain size L is normally much larger than ξ and the structure size D can basically be anything between ξ and L. If D is also much larger than ξ it will be very difficult to resolve the physical value of ξ numerically. For example, for a droplet with a diameter of 1 mm and an interfacial thickness of 0.1 nm the ratio of the structure size and the interfacial thickness D/ξ equals 10^7. If we use a homogeneously spaced numerical grid, assuming we need at least 2 grid points to be able to

capture the interface, we will need about $4 \cdot 10^{14}$ grid points in two dimensions and $8 \cdot 10^{21}$ in three dimensions to capture the droplet with the interface. Calculations on these mesh sizes are either impossible or very cumbersome using currently available computer resources. Even when using more sophisticated numerical techniques such as adaptive re-meshing, still too many levels of refinement are needed to capture the interface. In this thesis we therefore focus on the question whether it is possible to use a numerically acceptable size for the interfacial thickness instead of the real value and still get sufficiently accurate and physically correct results.

In chapter 2 the diffuse-interface method will be presented in detail and it will be shown how the coupling with the equations of fluid dynamics is made. In chapter 3 we show some basic results of the diffuse-interface approach, explaining the basic features of the method. We consider phase separation (nucleation and spinodal decomposition) in one- and two-dimensional systems and interfacial instabilities in a Hele-Shaw geometry. In the next two chapters we focus on the question whether we can use a computational interfacial thickness which is much larger than the real physical value and still get physically correct and accurate results. In chapter 4 we consider 1 flow and instabilities in a Hele-Shaw cell. The computational diffuse-interface results are directly compared to analytical, sharp-interface results for thermo-capillary flow. We investigate how the results depend on the choice of the interfacial thickness. Chapter 5 deals with coalescence in hyperbolic flows. We again investigate the dependence on the choice of the interfacial thickness. Finally, chapter 6 contains some conclusions and recommendations.

Chapter 2

A DIFFUSE-INTERFACE THEORY FOR MULTICOMPONENT FLUID SYSTEMS

2.1 Introduction

In this chapter we will describe the diffuse-interface theory in detail. The system which we will consider in this chapter is a closed volume V with boundary S containing an inhomogeneous mixture of N fluids.

As mentioned in chapter 1, the essential ingredient of diffuse-interface theories is the non-local effect in the free energy of the system. In section 2.2 a lattice model is used to show how molecular interactions can give rise to non-local energy effects in binary fluids. Next, the discrete lattice model is replaced by a more sophisticated continuous representation of the non-local internal energy, in the spirit of van der Waals (1979). We show how a diffuse-interface theory can be constructed, using a Taylor expansion of the density. Section 2.3 is devoted to the Cahn-Hilliard theory (Cahn and Hilliard, 1958), which is based on a Taylor expansion of the Helmholtz free energy density about the homogeneous state.

In sections 2.2 and 2.3 we only consider quiescent systems. However, to be able to model mechanically induced structure development we have to include convection. Sections 2.4 to 2.6 are devoted to coupling the equations of hydrodynamics and the diffuse-interface approach. In section 2.4 we first write down the local balance equations for mass, mass fraction, momentum and energy, by considering an arbitrary volume Ω within V. The local balance equations do not form a complete set of equations: the diffusion, momentum and energy flux appearing in the local balance equations need to be specified. In sections 2.5 and 2.6, non-classical expressions for the reversible and dissipative parts of the fluxes will be derived following the principles of classical irreversible thermodynamics (de Groot and Mazur, 1984). Finally, in section 2.7 we consider isothermal systems, for which the individual components are incompressible and in section 2.8, we briefly discuss polymer systems.

2.2 Background

Consider an inhomogeneous, binary fluid within a closed volume V with boundary S, as depicted in figure 2.1. The fluids are labelled $i, j = 1, 2$. A small, planar piece of the

interface is represented by a lattice. Each site of the lattice, labelled A, $B = 1 \ldots \mathcal{N}$, is either occupied by fluid 1 (black) or fluid 2 (white). In general, a site i interacts with all other sites.
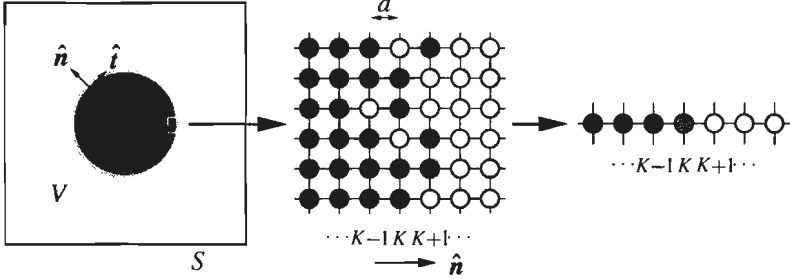
Figure 2.1: lattice model of a fluid-fluid interface.

The interaction energy of a site A can be written as

$$U_A = - \sum_{i,j=1}^{2} \sum_{\substack{B=1 \\ B \neq A}}^{\mathcal{N}} \varepsilon_{ij}^{AB} \phi_i^A \phi_j^B , \tag{2.1}$$

where ε_{ij}^{AB} is the interaction energy: for example, ε_{12}^{AB} is the interaction energy between site A occupied by fluid 1 and site B occupied by fluid 2. The site occupation variable ϕ_1^A equals 1 if site A is occupied by fluid 1 and zero otherwise. A common assumption in lattice modelling is that only neighbour interactions contribute to the total interaction energy (Doi, 1996). In figure 2.1 the nearest neighbours are connected by lines: each site has four nearest neighbours. If only the nearest neighbour interactions are taken into account, the sum over the sites B in equation (2.1) can be replaced by the sum over nearest neighbours of site A and ε_{ij}^{AB} can be replaced by the nearest neighbour interaction energy ε_{ij}. Since the density varies only in the direction normal to the interface, we also assume that there is a uniform distribution in each column K (see figure 2.1) and we replace the site occupation variable of a site A in column K by its average value $\bar{\phi}$. The interaction energy of a site A in column K can now be written as

$$U_{K(A)} = - \sum_{i,j=1}^{2} [(z - 2z')\varepsilon_{ij}\bar{\phi}_i^K \bar{\phi}_j^K + z'\varepsilon_{ij}\bar{\phi}_i^K (\bar{\phi}_j^{K+1} + \bar{\phi}_j^{K-1})] , \tag{2.2}$$

where z is the number of nearest neighbours, z' is the number of nearest neighbours in the neighbouring column. Collecting the z'-terms in equation (2.2), we obtain

$$U_{K(A)} = - \sum_{i,j=1}^{2} [z\varepsilon_{ij}\bar{\phi}_i^K \bar{\phi}_j^K + z'\varepsilon_{ij}\bar{\phi}_i^K (\bar{\phi}_j^{K+1} - 2\bar{\phi}_j^K + \bar{\phi}_j^{K-1})] . \tag{2.3}$$

The first term on the right hand side represents the homogeneous part of the interaction energy. The second term has got a non-local character. The term inside the brackets, $\bar{\phi}_j^{K+1} -$

$2\bar{\phi}_j^{K+1}+\bar{\phi}_j^{K-1}$, can be identified as the discrete second order spatial derivative. That is, by replacing $\bar{\phi}^K$ by its continuous equivalent $\phi(r)$, we can write the continuous three dimensional analogue of equation (2.3) as

$$U(r) = -\sum_{i,j=1}^{2}[z\varepsilon_{ij}\phi_i\phi_j + z'\varepsilon_{ij}\phi_i a^2\nabla^2\phi_j]\,, \tag{2.4}$$

where a is the distance between two neighbouring sites. Dividing by a^3 we can define the energy density

$$u(r) = -n_0 \sum_{i,j=1}^{2}[\varepsilon_{ij}\phi_i\phi_j + \frac{1}{6}\varepsilon_{ij}\phi_i a^2\nabla^2\phi_j]\,, \tag{2.5}$$

where we used $n_0 = z/a^3$ and $z/z' = 6$ (cubic lattice). Integrating $u(r)$ over the volume V yields the total internal energy. Assuming the ε_{ij}'s are constant, we obtain after partial integration

$$\mathcal{U}[\phi, \nabla\phi] = n_0 \int_V [u_0(\phi) + \frac{1}{6}a^2\varepsilon(\nabla\phi)^2]\,d^3r\,, \tag{2.6}$$

where $\phi = \phi_i = 1 - \phi_j$, $\varepsilon = \varepsilon_{ii} + \varepsilon_{jj} - 2\varepsilon_{ij}$ and $u_0(\phi) = \varepsilon\phi(1-\phi) - \varepsilon_{ii}\phi - \varepsilon_{jj}(1-\phi)$. We have also assumed that $\nabla\phi$ vanishes at the boundary of V. By subtracting the entropy term we can write the Helmholtz free energy $\mathcal{F}$ as

$$\mathcal{F}[\phi, \nabla\phi] = \mathcal{U}[\phi, \nabla\phi] - TS[\phi] = n_0 \int_V [f_0(\phi) + \frac{1}{6}a^2\varepsilon(\nabla\phi)^2]\,d^3r\,, \tag{2.7}$$

where T is the temperature and S is the entropy. It is assumed that there are no non-local effects in the entropy. For small-molecule systems this is a valid approximation. In polymer systems, however, the conformational entropy, which is associated with the various directions in which each bond can point, also has a non-local character, which can easily dominate the non-local effects in the internal energy (Helfand, 1982). We will discuss polymer systems in more detail in section 2.8.

The lattice model is a very simple representation of the system. The continuous version of the Helmholtz free energy, equation (2.7), was derived using the assumption that only nearest neighbour interactions in the lattice contribute to the total interaction energy. However, in most systems the distribution of the molecules is not according to the lattice: there is a density distribution which is determined by the interaction energy. In this spirit, a more sophisticated representation of the discrete Helmholtz free energy, which is given by $F = -TS + \sum_A U_A$, can be written as a function of the density distribution (Evans, 1979):

$$\mathcal{F}[n_1, n_2] = -TS[n_1, n_2] - \frac{1}{2}\sum_{i,j=1}^{2}\iint_V \varepsilon_{ij}(|r - r'|)n_{ij}^{(2)}(r, r'; \varepsilon_{ij})\,d^3r\,d^3r'\,, \tag{2.8}$$

where n_i is the number density of fluid i and $n_{ij}^{(2)}$ is the pair distribution function, which is related to the individual density fields as

$$n_{ij}^{(2)}(r, r'; \varepsilon_{ij}) = n_i(r) n_j(r') g_{ij}^{(2)}(r, r'; \varepsilon_{ij}) , \tag{2.9}$$

with $g_{ij}^{(2)}$ the pair correlation function. To evaluate this functional one needs to specify the pair correlation function. However, for inhomogeneous fluids this function is not known. Very often it is set equal to unity, which is known as the random phase approximation Evans (1979). We will return to this point in the next section.

The chemical potential μ_i of component i is defined as the change in $\mathcal{F}$ upon addition of an amount of component i, keeping temperature, volume and other density distributions $n_{j \neq i}$ fixed. In classical (homogeneous) thermodynamics it is not important where the amount of component i is added. For inhomogeneous fluids, on the other hand, the change in $\mathcal{F}$ does depend on where the amount of component i is added. Mathematically, this is represented by functional differentiation of $\mathcal{F}$

$$\mu_i(r) = \frac{\delta \mathcal{F}}{\delta n_i} = \lim_{\delta V. \delta n_i \to 0} \frac{\mathcal{F}[n_i + \delta n_i, n_{j \neq i}] - \mathcal{F}[n_1, n_2]}{\int_{\delta V} \delta n_i \, d^3 r} . \tag{2.10}$$

Even though the chemical potential is a function of position in general, it can be shown that, in equilibrium, the chemical potential is constant everywhere in the fluid (Davis and Scriven, 1982). The equilibrium condition can be expressed as

$$\mu_i^{\text{eq}} = \left. \frac{\delta \mathcal{F}}{\delta n_i} \right|_{n^{\text{eq}}} . \tag{2.11}$$

This equation allows computation of equilibrium density profiles. The equations for the chemical potential are integral equations. The mass flux of a component is related to the gradient of its chemical potential. This means that the local mass balance equation for one of the components becomes an integro-differential equation, which is often difficult to deal with. Ending up with an integral form for the chemical potential can be avoided using the gradient density approach. The densities $n_j(r')$ are replaced by their Taylor expansions about r

$$n_j(r') = n_j(r) + \nabla n_j(r) \cdot (r - r') + \frac{1}{2} \nabla \nabla n_j(r) : (r - r')(r - r') + \dots . \tag{2.12}$$

The use of this Taylor expansion changes the mathematical structure of the energy functional (2.8). The non-local character is now represented by the local values of the density gradients rather than the non-local values of the density itself. The resulting equation can be written in the same mathematical form as equation (2.7)

$$\mathcal{F}[n_1, n_2, \nabla n_1, \nabla n_2] = \int_V f(n_1, n_2, \nabla n_1, \nabla n_2) \, d^3 r . \tag{2.13}$$

The chemical potential, defined by equation (2.10), can now be written as

$$\mu_i(r) = \frac{\delta \mathcal{F}}{\delta n_i} = \frac{\partial f}{\partial n_i} - \nabla \cdot \frac{\partial f}{\partial \nabla n_i} , \tag{2.14}$$

which has the differential form desired.

This relation for the chemical potential still needs the pair correlation function for the inhomogeneous system as input. In the next section we will show how we can avoid this.

2.3   Cahn-Hilliard theory

Another way to approximate the free energy functional $\mathcal{F}$, without ending up with an integral expression for the chemical potential, is to use a Taylor expansion of the free energy density f about the homogeneous state. This approach was used by Cahn and Hilliard (1958) and is different from the gradient density approach presented in the previous section: the Cahn-Hilliard theory, also called gradient free energy theory, does not need the inhomogeneous correlation function as input. As we shall see, the input required for the Cahn-Hilliard approach consists of the Helmholtz free energy density and the two-body direct correlation function of the homogeneous fluid, which both are well defined and experimentally accessible properties.

For an N-component fluid the Taylor expansion of the free energy density f about the homogeneous state f_0 can be written as

$$f(\{n_i\}, \{\nabla n_i\}, \{\nabla\nabla n_i\}, \dots) = f_0(\{n_i\}) + \sum_{i=1}^{N} \lambda_i \cdot \nabla n_i$$
$$+ \sum_{i=1}^{N} \kappa_i^{(1)} : \nabla\nabla n_i + \sum_{i,j=1}^{N} \frac{1}{2}\kappa_{ij}^{(2)} : \nabla n_i \nabla n_j + \dots ,$$

(2.15)

where $\{n_i\} = \{n_1, n_2, \dots, n_N\}$. The coefficients λ_i are zero, because the free energy is invariant under reflection ($r \rightarrow -r$). Furthermore, isotropy of the homogeneous system demands isotropy of the coefficients $\kappa_i^{(1)}$ and $\kappa_{ij}^{(2)}$

$$\kappa_i^{(1)} = \kappa_i^{(1)} \mathbf{I}, \quad \text{with} \quad \kappa_i^{(1)} = \left.\frac{\partial f}{\partial \nabla^2 n_i}\right|_0 \tag{2.16}$$

$$\kappa_{ij}^{(2)} = \kappa_{ij}^{(2)} \mathbf{I}, \quad \text{with} \quad \kappa_{ij}^{(2)} = \left.\frac{\partial^2 f}{\partial \nabla n_i \partial \nabla n_j}\right|_0 . \tag{2.17}$$

Consequently, we obtain

$$f = f_0 + \sum_{i=1}^{N} \kappa_i^{(1)} \nabla^2 n_i + \sum_{i,j=1}^{N} \frac{1}{2}\kappa_{ij}^{(2)} \nabla n_i \cdot \nabla n_j . \tag{2.18}$$

The total free energy $\mathcal{F}$ can now be written as

$$\mathcal{F} = \int_V f \, d^3r = \int_V \left(f_0 + \sum_{i,j=1}^{N} \frac{1}{2}\epsilon_{ij} \nabla n_i \cdot \nabla n_j\right) d^3r + \int_S \sum_{i=1}^{N} \kappa_i^{(1)} \nabla n_i \cdot \mathbf{n} \, d^2r , \tag{2.19}$$

where $\epsilon_{ij} = \kappa_{ij}^{(2)} - \partial\kappa_i^{(1)}/\partial n_j$. The second integral on the right hand side is a boundary integral which equals zero for vanishing density gradients at the boundary. Using statist-ical thermodynamics, it can be shown that the coefficients ϵ_{ij} can be written as (Davis and Scriven, 1982)

$$\epsilon_{ij} = \frac{k_B T}{6} \int_0^\infty r^2 C_{0.ij}^{(2)}(r; \{n_i\}) dr , \qquad (2.20)$$

where $C_0^{(2)}$ is the two-body direct correlation function of the homogeneous system and r is an integration parameter. Hence, as mentioned above, the required input for the gradient free energy theory is the free energy density and the two-body direct correlation function of the homogeneous fluid.

The chemical potential of component i is again defined by equation (2.14)

$$\mu_i = \frac{\partial f}{\partial n_i} - \nabla \cdot \frac{\partial f}{\partial \nabla n_i} = \frac{\partial f_0}{\partial n_i} + \sum_{j.k=1}^N \frac{\partial \epsilon_{jk}}{\partial n_i} \nabla n_j \cdot \nabla n_k - \sum_{k=1}^N \nabla \cdot (\epsilon_{ik} \nabla n_k) , \qquad (2.21)$$

where we used the fact that the coefficients ϵ_{ij} may depend on the densities $\{n_i\}$. In non-equilibrium, a gradient in the chemical potential will cause mass diffusion. Assuming that the diffusion flux is a linear combination of all chemical potential gradients, we can write mass conservation for component i as

$$\frac{\partial n_i}{\partial t} = -\nabla \cdot \sum_{k=1}^N L_{ik} \nabla \mu_k , \qquad (2.22)$$

where the L_{ik}'s are the mobility parameters. This equation is known as the Cahn-Hilliard equation. Cahn (1964) has used this relation to model spinodal decomposition. Due to the truncation of the gradient expansion at the second order the Cahn-Hilliard theory was origin-ally thought to be only valid for the initial stages of spinodal decomposition or for near-critical systems, where density gradients are small. However, equation (2.19) is generally assumed to be also valid when concentration gradients are large (Kikuchi and Cahn, 1962; Elliot, 1989).

Up till now we did not include velocity, which is obviously essential if we want to model processes such as coalescence and break-up. In the next section we will, therefore, first write down the local balance equations for mass, momentum and energy for a system with an arbitrary velocity field $\boldsymbol{v}$.

2.4   Local balance equations

Consider an arbitrary volume element Ω within V, with boundary Γ and outer normal $\boldsymbol{n}$. The total mass of component i within Ω is

$$\mathcal{M}_i = \int_\Omega \rho_i \, d^3 \boldsymbol{r} . \qquad (2.23)$$

For chemically inert mixtures $\mathcal{M}_i$ can only change by a flux across the boundary Γ. Therefore

$$\frac{d\mathcal{M}_i}{dt} = \int_\Omega \frac{\partial \rho_i}{\partial t} d^3r + \int_\Gamma \rho_i v_i \cdot n \, d^2r = 0 , \tag{2.24}$$

where v_i is the velocity field of component i. Gauss' theorem can be used to transform the boundary integral into a volume integral. The resulting volume integral holds for an arbitrary volume element, therefore

$$\frac{\partial \rho_i}{\partial t} + \nabla \cdot (\rho_i v_i) = 0 . \tag{2.25}$$

Conservation of total mass follows from summing equation (2.25) over all components. This yields

$$\frac{\partial \rho}{\partial t} + \nabla \cdot (\rho v) = 0 , \tag{2.26}$$

where ρ is the density of the mixture

$$\rho = \sum_{i=1}^{N} \rho_i \tag{2.27}$$

and v is the barycentric velocity

$$v = \sum_{i=1}^{N} c_i v_i , \quad \text{with mass fraction} \quad c_i = \rho_i/\rho . \tag{2.28}$$

We can also define the velocities w_i relative to the barycentric velocity

$$w_i = v_i - v . \tag{2.29}$$

These velocities are called diffusion velocities. Combining (2.29) and (2.25) yields

$$\frac{\partial \rho_i}{\partial t} + \nabla \cdot (\rho_i v) = -\nabla \cdot (j_i) , \tag{2.30}$$

where $j_i = \rho_i w_i$ is the diffusion mass flow per unit area per unit time. Summing this equation over all components we should again obtain equation (2.26), therefore

$$\sum_{i=1}^{N} \rho_i w_i = 0 . \tag{2.31}$$

This shows that only $N-1$ of the diffusion velocities are independent. Instead of using the N independent velocities v_i we can also use the barycentric velocity and the $N-1$ independent diffusion velocities as set of independent variables.

The momentum $\mathcal{P}$ of a volume element can change due to contact and body forces. The equation of motion for Ω reads

$$\frac{d\mathcal{P}}{dt} = \frac{d}{dt} \int_\Omega \rho v \, d^3r = \int_\Gamma \tau \cdot n \, d^2r + \int_\Omega \rho f^{\text{ex}} \, d^3r \, , \tag{2.32}$$

where τ is the extra stress tensor and ρf^{ex} is the total external force density, defined by

$$\rho f^{\text{ex}} = \sum_{i=1}^N \rho_i f_i^{\text{ex}} \, . \tag{2.33}$$

The same arguments as used for mass balance result in the following local momentum balance equation[1]

$$\frac{\partial \rho v}{\partial t} + \nabla \cdot (\rho v v) = \nabla \cdot \tau + \rho f^{\text{ex}} \, . \tag{2.34}$$

Using local mass balance (2.26) this can be rewritten as

$$\rho \frac{dv}{dt} = \nabla \cdot \tau + \rho f^{\text{ex}} \, , \tag{2.35}$$

where $d/dt = \partial/\partial t + v \cdot \nabla$.

In the absence of heat sources the first law of thermodynamics for an open system states that the change in the sum of kinetic and internal energy $(d\mathcal{E})$ equals the work done by contact and body forces $(d\mathcal{W})$ plus the total energy flux $(d\mathcal{Q})$. That is

$$\frac{d\mathcal{E}}{dt} = \frac{d\mathcal{W}}{dt} + \frac{d\mathcal{Q}}{dt} \, , \tag{2.36}$$

where $\mathcal{E}$, being the sum of the internal energy $\mathcal{U}$ and the kinetic energy $\mathcal{K}$, can be written as

$$\mathcal{E} = \mathcal{U} + \mathcal{K} = \sum_{i=1}^N \int_\Omega \rho_i (u_i + \frac{1}{2} v_i \cdot v_i) \, d^3r \, , \tag{2.37}$$

with u_i the specific internal energy of component i and v_i the velocity field of component i. Using equations (2.28) and (2.31), $\mathcal{E}$ can be rewritten as

$$\mathcal{E} = \int_\Omega \rho (u + \frac{1}{2} v \cdot v) \, d^3r \, , \tag{2.38}$$

where

$$u = \sum_{i=1}^N (c_i u_i + \frac{1}{2} c_i w_i \cdot w_i) \equiv \tilde{u} + \frac{1}{2} \sum_{i=1}^N c_i w_i \cdot w_i \, . \tag{2.39}$$

---

[1] We only consider momentum conservation for the mixture here. It may be asked if the equations of motion exist for each component. Bearman and Kirkwood (1958) have shown, using statistical mechanics, that such equations do exist and that the sum of these equations can be written in the form of equation (2.34).

The second term on the right hand side is the kinetic energy of diffusion and $\tilde{u}$ is the 'true' internal energy, in the equilibrium sense. However, in most cases, the kinetic energy of diffusion can be neglected (de Groot and Mazur, 1984). In the sequel we will use the approximation $u = \tilde{u}$. The performed work and the energy flux can be written as

$$\frac{dW}{dt} = \int_\Gamma \tau \cdot v \cdot n \, d^2r + \sum_{i=1}^{N} \int_\Omega \rho_i f_i^{ex} \cdot v \, d^3r \,, \tag{2.40}$$

$$\frac{dQ}{dt} = -\int_\Gamma q \cdot n \, d^2r \,. \tag{2.41}$$

The resulting local energy balance equation is

$$\rho \frac{d}{dt}(u + \frac{1}{2}v \cdot v) = \nabla \cdot (\tau \cdot v) - \nabla \cdot q + \rho f^{ex} \cdot v + \sum_{i=1}^{N} f_i^{ex} \cdot \rho_i w_i \,. \tag{2.42}$$

Mass and momentum conservation can be used to single out the kinetic contribution to equation (2.42). This results in

$$\rho \frac{du}{dt} = \tau : \nabla v - \nabla \cdot q + \sum_{i=1}^{N} f_i^{ex} \cdot \rho_i w_i \,. \tag{2.43}$$

In this thesis we will only use gravity f_g as an external force, which is the same for each component. In this case the last term on the right hand side equals zero.

In summary, the local balance equations for mass, momentum and energy in a gravity field are

$$\frac{d\rho}{dt} = -\rho \nabla \cdot v \,, \tag{2.44}$$

$$\rho \frac{dc_i}{dt} = -\nabla \cdot j_i \,, \tag{2.45}$$

$$\rho \frac{dv}{dt} = \nabla \cdot \tau + \rho f_g \,, \tag{2.46}$$

$$\rho \frac{du}{dt} = \tau : \nabla v - \nabla \cdot q \,. \tag{2.47}$$

To complete this set of equations we need additional equations for the mass, momentum and energy flux, j_i, τ and q respectively. To this end we follow the phenomenological approach of classical irreversible thermodynamics (de Groot and Mazur, 1984), which states that the fluxes are linear functions of the thermodynamic forces appearing in the entropy production σ. The entropy production appears in the local balance equation for the entropy s, which can be written as

$$\rho \frac{ds}{dt} = -\nabla \cdot j_s + \sigma \,. \tag{2.48}$$

This equation states that the entropy of a volume element can change because of entropy in- and outflow, represented by the entropy flux j_s, and because of irreversible processes taking place within the element, represented by the entropy production σ. According to the second law of thermodynamics σ has to be non-negative

$$\sigma \geq 0 . \tag{2.49}$$

For reversible transitions or systems in equilibrium $\sigma = 0$. To find a more explicit expression for σ we need to relate changes in the entropy to changes in the other properties appearing in the other local balance equations. This can be done by considering the Gibbs relation.

2.5   Gibbs relation

From classical thermodynamics it is known that, for a homogeneous system in equilibrium, the internal energy is a function of the entropy s and the densities ρ_i. Here we consider inhomogeneous fluids. In the spirit of the equilibrium diffuse-interface theory, presented in sections 2.2 and 2.3, the internal energy u is also a function of density gradients

$$u = u(s, \{\rho_i\}, \{\nabla \rho_i\}) . \tag{2.50}$$

The total differential of this equation is

$$du = \frac{\partial u}{\partial s} ds + \sum_{i=1}^{N} \frac{\partial u}{\partial \rho_i} d\rho_i + \sum_{i=1}^{N} \frac{\partial u}{\partial \nabla \rho_i} \cdot d\nabla \rho_i , \tag{2.51}$$

where the partial differentiations are such that all other independent variables are kept constant. Using the thermodynamic relation $\partial \tilde{u}/\partial s = T$, equation (2.51) can be rewritten as a non-classical Gibbs relation

$$T ds = du - \sum_{i=1}^{N} \frac{\partial u}{\partial \rho_i} d\rho_i - \sum_{i=1}^{N} \frac{\partial u}{\partial \nabla \rho_i} \cdot d\nabla \rho_i . \tag{2.52}$$

To be able to couple the Gibbs relation to the local balance equations of the previous section we have to write it in a local form. To write it in a local form we now assume that, even though the total system is necessarily in equilibrium, the Gibbs relation remains valid for a volume element travelling with the barycentric velocity v. This approximation is also called the local equilibrium approximation (de Groot and Mazur, 1984).

$$T \frac{ds}{dt} = \frac{du}{dt} - \sum_{i=1}^{N} \frac{\partial u}{\partial \rho_i} \frac{d\rho_i}{dt} - \sum_{i=1}^{N} \frac{\partial u}{\partial \nabla \rho_i} \cdot \frac{d\nabla \rho_i}{dt} . \tag{2.53}$$

Using the local mass balance equations (2.44) and (2.45) this equation can be rewritten as

$$T \frac{ds}{dt} = \frac{du}{dt} - \frac{p_o}{\rho^2} \frac{d\rho}{dt} - \sum_{i=1}^{N} \mu_{oi} \frac{dc_i}{dt} - \sum_{i=1}^{N} \frac{\partial u}{\partial \nabla \rho_i} \cdot \frac{d\nabla \rho_i}{dt} , \tag{2.54}$$

where the homogeneous part of the chemical potential and the pressure are given by

$$\mu_{oi} = \frac{\partial \rho u}{\partial \rho_i} - Ts \quad \text{and} \quad p_o = \sum_{i=1}^{N} \rho_i \mu_{oi} - \rho u + \rho Ts , \tag{2.55}$$

respectively. For a detailed derivation of equations (2.54) and (2.55) see appendix A.

The gradient term in equation (2.54) still needs to be evaluated. An expression for $d\nabla \rho_i / dt$ can be found by taking the gradient of the local mass balance equation for component i. After some manipulations we find

$$\frac{d\nabla \rho_i}{dt} = -\nabla v \cdot \nabla \rho_i - \nabla(\rho_i \nabla \cdot v) - \nabla\nabla \cdot j_i . \tag{2.56}$$

We can now combine equations (2.54) and (2.47). Using local mass balance together with the identities $\nabla \cdot v = I : \nabla v$ and

$$\frac{\partial u}{\partial \nabla \rho_i} \cdot \nabla v \cdot \nabla \rho_i = \frac{\partial u}{\partial \nabla \rho_i} \nabla \rho_i : \nabla v \tag{2.57}$$

we obtain

$$\rho T \frac{ds}{dt} = (\tau - \tau_r) : \nabla v - \nabla \cdot (q - q_r - q_d) + \sum_{i=1}^{N} \mu_i \nabla \cdot j_i , \tag{2.58}$$

with

$$\tau_r = -pI - \sum_{i=1}^{N} \frac{\partial \rho u}{\partial \nabla \rho_i} \nabla \rho_i , \tag{2.59}$$

$$q_r = \sum_{i=1}^{N} \frac{\partial \rho u}{\partial \nabla \rho_i} \rho_i \nabla \cdot v , \tag{2.60}$$

$$q_d = \sum_{i=1}^{N} \frac{\partial \rho u}{\partial \nabla \rho_i} \nabla \cdot j_i , \tag{2.61}$$

$$\mu_i = \frac{\partial \rho u}{\partial \rho_i} - \nabla \cdot \frac{\partial \rho u}{\partial \nabla \rho_i} - Ts , \tag{2.62}$$

$$p = \sum_{i=1}^{N} \rho_i \mu_i - \rho u + \rho Ts . \tag{2.63}$$

Note that μ_i has the same mathematical form as the chemical potential in sections 2.2 and 2.3, which was obtained by variational differentiation of the free energy functional.

To find an expression for the entropy production σ, equation (2.58) has to be rewritten in the form of equation (2.48). Dividing equation (2.58) by T and rearranging the terms we obtain

$$\rho \frac{ds}{dt} = -\nabla \cdot j_s + \sigma , \tag{2.64}$$

with

$$j_s = \frac{1}{T}\left(q - q_r - q_d - \sum_{i=1}^{N} \mu_i j_i\right),\tag{2.65}$$

$$\sigma = \frac{1}{T}(\tau - \tau_r):\nabla v + (q - q_r - q_d)\cdot\nabla\frac{1}{T} - \sum_{i=1}^{N} j_i\cdot\nabla\frac{\mu_i}{T}.\tag{2.66}$$

The entropy production has a simple structure: it is the sum of the products of the thermo-dynamics fluxes and forces. In equilibrium both fluxes and forces vanish. The equilibrium relations are therefore given by

$$j_i = 0, \quad \tau = \tau_r \text{ and } q = q_r.\tag{2.67}$$

Here we have identified τ_r and q_r as the reversible parts of the stress tensor and the energy flux, respectively. Besides the isotropic pressure contribution, there is also an anisotropic contribution to τ_r, which depends on the density gradients. This means that, at an interface between two fluids, the tangential stress is not equal to the normal stress. We shall see later on that this difference is closely related to the interfacial tension.

To find phenomenological relations for the thermodynamic fluxes we have to consider the dissipative part of the entropy production.

2.6   Phenomenological equations

In this section we will derive the phenomenological equations for the thermodynamic fluxes, using the principle of classical irreversible thermodynamics (de Groot and Mazur, 1984): the fluxes are assumed to be linear functions of the independent forces appearing in the entropy production. To write the entropy production as a linear combination of independent fluxes and forces we have to split up the first term on the right hand side of equation (2.66) in a deviatoric and a diagonal part.

$$\sigma = \frac{1}{T}\tau_v^d:\nabla_d v + \frac{1}{3T}\text{Tr}(\tau_v)\nabla\cdot v + q_h\nabla\frac{1}{T} - \sum_{i=1}^{N} j_i\cdot\nabla\frac{\mu_i}{T} > 0,\tag{2.68}$$

where $\tau_v = \tau - \tau_r$ is the viscous stress tensor and $q_h = q - q_r - q_d$ is the heat flux, Tr is the trace operator and τ_v^d and $\nabla_d v$ are the deviatoric parts of τ_v and ∇v, respectively. By splitting up the viscous term in a deviatoric and a diagonal part we separate the contribution of shear viscosity and bulk viscosity.

We now assume that the fluxes are linear functions of the independent forces appearing in (2.68). Keeping in mind that fluxes and forces of different tensorial character can not couple,

we obtain the following phenomenological relations

$$\tau_v^d = \frac{\Lambda_s}{2T}[\nabla v + \nabla v^\mathsf{T} - \frac{2}{3}\nabla \cdot v \, \mathsf{I}]\,, \tag{2.69}$$

$$\frac{1}{3}\mathrm{Tr}(\tau_v) = \frac{\Lambda_b}{T}\nabla \cdot v\,, \tag{2.70}$$

$$q_h = \Lambda_{qq}\nabla\frac{1}{T} + \sum_{k=1}^{N-1}\Lambda_{qk}\nabla\left(\frac{\mu_k - \mu_N}{T}\right)\,, \tag{2.71}$$

$$j_i = \Lambda_{iq}\nabla\frac{1}{T} + \sum_{k=1}^{N-1}\Lambda_{ik}\nabla\left(\frac{\mu_k - \mu_N}{T}\right)\,. \tag{2.72}$$

We have assumed that the viscous stress tensor is symmetric and we used the fact that only $N - 1$ of the diffusion fluxes are independent. The total viscous stress tensor $\tau_v = \tau_v^d + \mathrm{Tr}(\tau_v)\mathsf{I}/3$ is the extra stress tensor and the coefficients $\Lambda_s/(2T)$ and Λ_b/T can be identified as the shear and bulk viscosity, respectively. The relations for q_h and j_i include so-called cross effects: the diffusion flux depends not only on the chemical potential gradients but also on the temperature gradient (thermo-diffusion or Soret effect) and the energy flux also depends on the chemical potential gradients (diffusion-thermo or Dufour effect).

The local balance equations: (2.44) to (2.47) and the phenomenological equations: (2.69) to (2.72), supplemented with the equations of state $u = u(\{\rho_i\}, \{\nabla\rho_i\}, T)$ and $p = p(\rho, T)$ now form a complete set of equations, which can be solved with the appropriate initial and boundary conditions.

2.7 Quasi-incompressible systems

So far we have considered non-isothermal, compressible systems. In this thesis, however, we are mainly concerned with incompressible, (nearly) isothermal systems. For an incompressible, isothermal fluid the density depends only on the mass fractions $\{c_i\}$. If there is no volume change upon mixing, the reciprocal density is a linear function of the mass fractions (Joseph and Renardy, 1993)

$$\frac{1}{\rho} = \sum_{i=1}^{N-1}\frac{c_i}{\varrho_i - \varrho_N} + \frac{1}{\varrho_N}\,, \tag{2.73}$$

where ϱ_i is the density of component i as a pure substance (not to be confused with ρ_i). Mixtures which obey equation (2.73) are called simple mixtures.

For incompressible systems, the internal energy is a function of $\{c_i\}$ rather than the densities $\{\rho_i\}$. That is

$$u = u(s, \{c_i\}, \{\nabla c_i\}) \qquad i = 1 \ldots N - 1\,. \tag{2.74}$$

This has some important consequences. The first one is that the pressure can not be defined as in section 2.5. On the other hand, as pointed out by Joseph and Renardy (1993), for a

mixture of individually incompressible fluids with different densities the density changes if the composition changes. Therefore, we still have a pressure-like effect, which is called quasi-compressibility and which is represented by the fact that the velocity field is not divergence free for such systems. More specifically, combining the local mass balance equations (2.44) and (2.45) using the simple mixture relation (2.73) we obtain

$$\nabla \cdot v = \sum_{i=1}^{N-1} \kappa_i \nabla \cdot j_i \quad \text{with} \quad \kappa_i = \frac{1}{\rho^2} \frac{\partial \rho}{\partial c_i} = \frac{1}{\varrho_N} - \frac{1}{\varrho_i} . \tag{2.75}$$

A second important consequence of equation (2.74) is that the structure of the entropy production changes. Not only because the time derivatives of $\{c_i\}$ and $\{\nabla c_i\}$ instead of $\{\rho_i\}$ and $\{\nabla \rho_i\}$ appear in the Gibbs relation now, but also because the divergence of the velocity field is no longer an independent thermodynamic force. This effect was also reported by Lowengrub and Truskinovsky (1998). The Gibbs relation for a quasi-incompressible system is (see appendix A)

$$T \frac{ds}{dt} = \frac{du}{dt} - \sum_{i=1}^{N-1} \frac{\partial u}{\partial c_i} \frac{dc_i}{dt} - \sum_{i=1}^{N-1} \frac{\partial u}{\partial \nabla c_i} \cdot \frac{d\nabla c_i}{dt} , \tag{2.76}$$

where dc_i/dt is given by equation (2.45) and

$$\frac{d\nabla c_i}{dt} = -\nabla v \cdot \nabla c_i - \nabla(\frac{1}{\rho} \nabla \cdot j_i) . \tag{2.77}$$

Combining the local energy balance equation (2.47) and the Gibbs relation (2.76) now yields

$$\rho T \frac{ds}{dt} = (\tau - \tau_r) : \nabla v - \nabla \cdot (q - q_d) + \sum_{i=1}^{N-1} (\mu_i - \mu_N) \nabla \cdot j_i , \tag{2.78}$$

with

$$\tau_r = -\rho \sum_{i=1}^{N-1} \frac{\partial u}{\partial \nabla c_i} \nabla c_i , \tag{2.79}$$

$$q_d = \rho \sum_{i=1}^{N-1} \frac{\partial u}{\partial \nabla c_i} \nabla \cdot j_i , \tag{2.80}$$

$$\mu_i - \mu_N = \frac{\partial u}{\partial c_i} - \frac{1}{\rho} \nabla \cdot (\rho \frac{\partial u}{\partial \nabla c_i}) . \tag{2.81}$$

As stated above, to find a correct expression for the entropy production in terms of independent forces and fluxes we have to include the fact that $\nabla \cdot v$ and $\nabla \cdot j_i$ are not independent. Using equation (2.75) and splitting up ∇v into a deviatoric part and a diagonal part we obtain

$$\rho T \frac{ds}{dt} = (\tau - \tau_r) : \nabla_d v - \nabla \cdot (q - q_d) + \sum_{i=1}^{N-1} (\mu_i^\bullet - \mu_N^\bullet) \nabla \cdot j_i , \tag{2.82}$$

where

$$\mu_i^\bullet - \mu_N^\bullet = \mu_i - \mu_N - \frac{1}{3}\kappa_i \mathrm{Tr}(\tau - \tau_r) \ . \tag{2.83}$$

The entropy production for an isothermal system is now given by

$$\sigma = \frac{1}{T}(\tau - \tau_r):\nabla_d v - \frac{1}{T}\sum_{i=1}^{N-1} j_i \cdot \nabla(\mu_i^\bullet - \mu_N^\bullet) \ . \tag{2.84}$$

The equilibrium relations are now

$$j_i = 0 \ \text{ and } \ \tau - \tau_r = -p\,\mathsf{I} \ , \tag{2.85}$$

with p is an arbitrary pressure field. The chemical potential difference $\mu_i^\bullet - \mu_N^\bullet$ can also be written as

$$\mu_i^\bullet - \mu_N^\bullet = \mu_i - \mu_N + \kappa_i p \ . \tag{2.86}$$

Using the same technique as in the previous section, neglecting bulk viscosity, we obtain the following phenomenological equations for the viscous stress tensor and the diffusion flux

$$\tau_v = \eta[\nabla v + \nabla v^\mathsf{T} - \frac{2}{3}\nabla \cdot v\,\mathsf{I}] \ , \tag{2.87}$$

$$j_i = \frac{1}{T}\sum_{k=1}^{N-1} \Lambda_{ik}\nabla(\mu_k^\bullet - \mu_N^\bullet) \ , \tag{2.88}$$

where η is the shear viscosity.

The local momentum balance equation (2.46) can now be written as

$$\rho\frac{dv}{dt} = -\nabla p - \nabla \cdot \sum_{i=1}^{N-1} \rho\frac{\partial u}{\partial \nabla c_i}\nabla c_i + \nabla \cdot \tau_v + \rho f_g \ . \tag{2.89}$$

We can make one further simplification concerning the gradient term in the momentum equation. The second term on the right hand side can be rewritten as (see appendix A)

$$-\nabla \cdot \sum_{i=1}^{N-1} \rho\frac{\partial u}{\partial \nabla c_i}\nabla c_i = -\rho\nabla f + \rho\sum_{i=1}^{N-1}(\mu_i - \mu_N)\nabla c_i \ , \tag{2.90}$$

where $f = u - Ts$ is the specific Helmholtz free energy. Adding the pressure term and dividing by ρ we obtain

$$-\frac{1}{\rho}\nabla p + \nabla f + \sum_{i=1}^{N-1} \mu_i\nabla c_i = -\nabla(f + \frac{p}{\rho}) + \sum_{i=1}^{N-1}(\mu_i^\bullet - \mu_N^\bullet)\nabla c_i \ . \tag{2.91}$$

Defining the specific Gibbs free energy as $g = f + p/\rho$, the momentum equation can now be written as

$$\frac{d\boldsymbol{v}}{dt} = -\nabla g + \sum_{i=1}^{N-1} (\mu_i^\bullet - \mu_N^\bullet)\nabla c_i + \frac{1}{\rho}\nabla\cdot\boldsymbol{\tau}_v + \boldsymbol{f}_g \; . \tag{2.92}$$

In summary: the local mass, mass fraction and momentum balance equations for an inhomogeneous, quasi-incompressible, isothermal fluid mixture are

$$\frac{d\rho}{dt} = -\rho\nabla\cdot\boldsymbol{v} \; , \tag{2.93}$$

$$\rho\frac{dc_i}{dt} = \frac{1}{T}\nabla\cdot\sum_{k=1}^{N-1} \Lambda_{ik}\nabla(\mu_k^\bullet - \mu_N^\bullet), \quad \mu_i^\bullet - \mu_N^\bullet = \frac{\partial f}{\partial c_i} - \frac{1}{\rho}\nabla\cdot(\rho\frac{\partial f}{\partial\nabla c_i}) + \kappa_i p \; , \tag{2.94}$$

$$\frac{d\boldsymbol{v}}{dt} = -\nabla g + \sum_{i=1}^{N-1} (\mu_i^\bullet - \mu_N^\bullet)\nabla c_i + \frac{1}{\rho}\nabla\cdot\eta[\nabla\boldsymbol{v} + \nabla\boldsymbol{v}^\mathsf{T} - \frac{2}{3}\nabla\cdot\boldsymbol{v}\,\mathsf{I})] + \boldsymbol{f}_g \; , \tag{2.95}$$

where we have replaced $\partial u/\partial c_i$ and $\partial u/\partial\nabla c_i$ by $\partial f/\partial c_i$ and $\partial f/\partial\nabla c_i$, respectively. To complete this set of equations we need equation (2.73), an equation which specifies the viscosity as a function of the mass fractions $\eta = \eta(\{c_i\})$ and an equation of state $f = f(T, \{c_i\}, \{\nabla c_i\})$. The Cahn-Hilliard free energy (2.19) can be used to specify the equation of state.

2.8 Polymer systems

In section 2.2 we already mentioned that polymer systems need some special attention. In polymer systems, conformational entropy, which is associated with the various directions in which each bond can point, also has a non-local character. Helfand (1982) showed that the ratio of the non-local internal energy and the non-local conformational entropy term can be estimated as $\chi\sigma^2/b^2$, where $\chi = \varepsilon/(k_B T)$ is a dimensionless measure of the interaction energy, σ is the monomer-monomer interaction length and b is the mean length of one segment in the polymer. This shows that for small values of χ, which is common in polymer systems, the non-local conformational entropy term dominates. The gradient density approach, presented in section 2.2, which only includes non-local effects in the internal energy, is therefore not valid for polymer systems.

In the Cahn-Hilliard approach, discussed in section 2.3, a Taylor expansion of the Helmholtz free energy density is used instead of a Taylor expansion of the density. The Helmholtz free energy also includes entropy. Therefore, one might expect that non-local effects in the conformational entropy can be included using the Cahn-Hilliard approach.

The first Cahn-Hilliard type model for polymer systems was proposed by Debye (1959). In this model the size of the polymer molecule, the radius of gyration, is used as the interaction length. However, Debye's model does not include non-local effects in the conformational entropy, because the deformability of the polymer chains is neglected. Therefore, as pointed

out by Helfand (1982), the Debye model can only be applied to dilute polymer solutions in which polymer deformability can be neglected, or to near-critical systems in which the correlation length exceeds the gyration radius of the polymer. In spite of these shortcomings, Debye's model is still widely used and successfully applied (e.g. Barton *et al.*, 1998).

A more sophisticated Cahn-Hilliard type model for polymer blends, which include non-local entropy effects, was proposed by de Gennnes (1980). For a binary, incompressible blend it can be written as

$$\frac{\mathcal{F}}{k_B T} = \int_V \left(f_{\text{FH}}(\phi) + \frac{b^2}{\lambda \phi (1 - \phi)} (\nabla \phi)^2 \right) d^3 r , \qquad (2.96)$$

where f_{FH} is the (homogeneous) Flory-Huggins free energy density, ϕ is the volume fraction of one of the components and b is the mean segment length. The second term in the integrand represent the non-local effects in the conformational entropy (the non-local internal energy describing the monomer-monomer interactions are neglected). In the weak segregation limit (de Gennes, 1977) the parameter λ equals 36 . In the strong segregation limit the functional form for the prefactor of the gradient term is only correct in the long chain limit and λ equals 24 in this case (Lifschitz and Freed, 1993).

The Cahn-Hilliard theory truncates the gradient expansion at the square gradient term. For the weak segregation limit this is a valid approximation. However, when the interfacial thickness becomes small compared to the radius of gyration, higher order terms should be included. Theories which include these higher order terms are for example the self-consistent field formalism studied by Helfand and Tagami (1972) and Helfand and Sapse (1976) or the density functional approach (Evans, 1979; McMullen, 1991). Helfand and Tagami (1972) studied the conformational statistics of a polymer chain in a chemical potential field created by other molecules in the system. The conformational statistics can be represented by a function $Q(r, \tau; r_0)$, which is proportional to the probability that a polymer chain of τ segments has one end at r_0 and the other end at r. For a polymer in a chemical potential field $\mu(r)$ created by other molecules Q satisfies a modified diffusion equation of the form

$$\frac{\partial Q}{\partial \tau} = \frac{b^2}{6} \nabla^2 Q - \frac{\mu}{k_B T} Q , \qquad (2.97)$$

where b is the mean length of a segment. The first term on the right hand has to be put in contrast with the non-local energy term appearing in the chemical potential. In the long chain limit the dependence of Q no longer depends on τ and an analytical solution for the interface profile and interfacial thickness can be found, which match the Cahn-Hilliard results. McMullen (1991) proposed a density functional theory for polymer-solvent systems. Using gradient expansions, he found the nonlinear gradient term appearing in the Cahn-Hilliard-de-Gennes theory as a limiting case of his theory, obtaining both the weak ($\lambda = 36$) and the strong segregation limit ($\lambda = 24$). McMullen found that for interfaces with a thickness large compared to the radius of gyration the Cahn-Hilliard-de-Gennes theory yields sufficiently accurate results for the interfacial thickness and tension.

2.9   Summary

In this chapter the diffuse-interface approach was discussed in detail. The essential ingredient of the diffuse-interface approach is the assumption that the specific internal energy not only depends on the entropy and the density but also on density gradients, or concentration gradients in case the fluids are incompressible. The density or concentration gradients are added as independent variables to the locally defined specific internal energy. Following the principles of irreversible thermodynamics non-classical expressions for the reversible and dissipative parts of the diffusion, momentum and energy flux were obtained.

The governing equations obtained for quasi-incompressible systems, equations (2.93), (2.94) and (2.95), will be used as a basis for the rest of this thesis. Exactly the same set of governing equations was derived by Lowengrub and Truskinovsky (1998) from a variational principle in which the Lagrangian takes the form

$$\mathcal{L} = \int\limits_{t_1}^{t_2} \int\limits_{\Omega} \rho(\tfrac{1}{2}|\boldsymbol{v}|^2 - f)\, d^3 r dt \,, \tag{2.98}$$

with $f = f(\rho, c, \nabla c)$. For compressible multi-component systems similar results were obtained by Blinowski (1975) using the same technique as used in this chapter. For density-matched fluids the model is also known as model H in the literature on critical phenomena (Gunton *et al.*, 1983; Hohenberg and Halperin, 1977).

The rest of this thesis is devoted to the application of the diffuse-interface model. Special attention will be paid to the question whether the model can be applied to large-scale systems in which the physical value of the interfacial thickness can not be captured numerically.

Chapter 3

THERMODYNAMIC AND HYDRODYNAMIC INSTABILITIES

3.1 Introduction

In this chapter we will show the basic features of the diffuse-interface model presented in chapter 2 by briefly discussing phase separation and interfacial instabilities. The systems considered in this chapter are simple systems, which allow us to study the basic features of diffuse-interface modelling separately. We do not show detailed results or compare to other results, rather we will then refer to the literature.

Section 3.2 is devoted to phase separation. First, we consider one-dimensional density-matched systems. In these systems, there are no effects of quasi-incompressibility or interfacial tension, which allows us to study phase separation without hydrodynamic coupling. In systems with a spatial dimension exceeding one, there is hydrodynamic coupling through curvature and interfacial tension. We show the effect of hydrodynamic coupling on spinodal decomposition in a two-dimensional system.

In section 3.3 we consider binary displacement flows in a Hele-Shaw cell, which consists of two closely spaced parallel plates. The systems considered are thermodynamically in equilibrium, but not in the mechanical sense: the interface becomes unstable if a more dense fluid is placed on top of a less dense one (Rayleigh-Taylor instability) or if a less viscous fluid is displacing a more viscous one (viscous fingering). A third kind of interfacial instability, caused by interfacial tension gradients (Marangoni instability) will be considered in the next chapter when we discuss thermo-capillary flow in more detail.

3.2 Phase separation

Consider an isothermal, density-matched, incompressible, binary fluid. In this case mass conservation (2.93) reduces to $\nabla \cdot v = 0$ and the local balance equation (2.94) for the mass fraction c of component 1 can be rewritten as

$$\frac{dc}{dt} = \frac{\Lambda}{\rho T}\nabla^2 \mu \quad \text{with} \quad \mu = \frac{\partial f}{\partial c} - \nabla \cdot (\frac{\partial f}{\partial \nabla c}) , \tag{3.1}$$

where we used $\mu = \mu_1 - \mu_2$ and we have assumed that the Onsager coefficient Λ is constant. In the spirit of the Cahn-Hilliard theory, presented in section 2.3, we assume that the specific Helmholtz free energy f can be written in the following form:

$$f(c, \nabla c) = f_0(c) + \frac{1}{2}\epsilon|\nabla c|^2 , \qquad (3.2)$$

where the gradient energy parameter $\epsilon = \epsilon_{11} + \epsilon_{22} - 2\epsilon_{12}$ is assumed to be constant. To complete the set of equations we need an additional equation of state, which specifies the homogeneous specific Helmholtz free energy f_0 as a function of c. A simple approximation for f_0 can be found by using a Taylor expansion of f_0 about the critical point $c = c_c$, which yields

$$f_0(\tilde{c}) = l(\tilde{c}) - \frac{1}{2}\alpha\tilde{c}^2 + \frac{1}{4}\beta\tilde{c}^4 , \qquad (3.3)$$

where $\tilde{c} = c - c_c$ is the reduced mass fraction and $l(\tilde{c})$ is a linear function of $\tilde{c}$. This approximation for f is also called the Ginzburg-Landau approximation (Gunton *et al.*, 1983). For example, for a regular solution (Prigogine, 1961) the specific Helmholtz free energy can be written as

$$f_0^{RS}(c) = \mu_1^0 c + \mu_2^0(1 - c) + RT[c \ln c + (1 - c)\ln(1 - c)] + \chi c(1 - c) , \qquad (3.4)$$

where μ_i^0 is the chemical potential of component i $(i = 1, 2)$ as a pure substance, R is the specific gas constant and χ is the interaction parameter. Expanding equation (3.4) about its critical point, $(c_c, T_c) = (\frac{1}{2}, \frac{1}{2}\chi/R)$, we obtain: $\alpha = 4R(T_c - T)$, $\beta = 16RT/3$ and $l(\tilde{c}) = l_0 + (\mu_1^0 - \mu_2^0)\tilde{c}$, where l_0 is a constant. This shows that, for isothermal systems, β is a positive constant and α is positive below the critical point and negative for temperatures exceeding the critical temperature T_c. Below the critical point, f_0 has the shape of a double well potential, as schematically depicted in figure 3.1. The chemical potential, as defined in
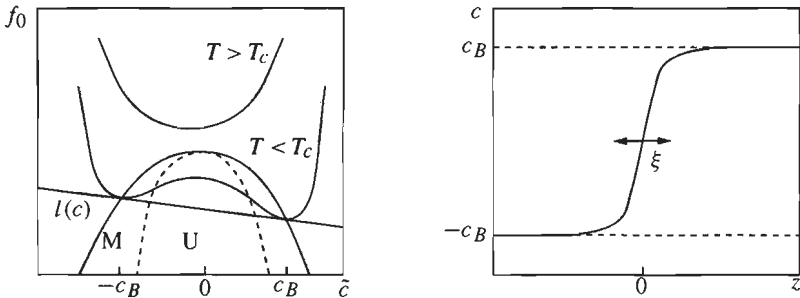

Figure 3.1: *Schematic picture of the homogeneous specific free energy f_0 as a function of c (left) and the equilibrium interface profile (right).*

(3.1), can now be written as

$$\mu = \mu^0 - \alpha\tilde{c} + \beta\tilde{c}^3 - \epsilon\nabla^2\tilde{c} , \qquad (3.5)$$

where $\mu^0 = \mu_1^0 - \mu_2^0$. For $\alpha > 0$ two possible equilibrium solutions are $\tilde{c} = \pm c_B$, with $c_B = \sqrt{\alpha/\beta}$. These two solutions represent the equilibrium bulk solutions, which correspond to the common tangent solutions of f_0 (left hand side of figure 3.1). However, there is another possible solution, which represents the interface profile. For a planar interface, located at $z = 0$, with z the direction normal to the interface, this solution is given by

$$\tilde{c}(z) = c_B \tanh\frac{z}{\sqrt{2}\xi}, \quad \text{with} \quad \xi = \sqrt{\frac{\epsilon}{\alpha}}, \tag{3.6}$$

where ξ is a measure for the interfacial thickness (right hand side of figure 3.1).

The time evolution of a non-equilibrium system is determined by equation (3.1). To write it in a non-dimensional form we use the following dimensionless variables: $\tilde{c}^* = \tilde{c}/c_B$, $\mu^* = \mu\xi^2/(\epsilon c_B)$, $z^* = z/\xi$ and $t^* = tD/\xi^2$, where $D = \Lambda\epsilon/(\rho T\xi^2)$. In dimensionless form, omitting the asterisk and the tilde notation, equation (3.1) now reads

$$\frac{\partial c}{\partial t} = \frac{\partial^2 \mu}{\partial z^2} \quad \text{with} \quad \mu = \mu^0 - c + c^3 - \frac{\partial^2 c}{\partial z^2}, \tag{3.7}$$

where we have assumed that there is no velocity, that is $dc/dt = \partial c/\partial t$. The unstable region below the critical point can be separated into two regions: the meta-stable region (M) and unstable region (U). In the meta-stable region the second order derivative of f_0 with respect to c, which is proportional to the diffusion coefficient, is positive, whereas it is negative in the unstable region. A system which is quenched into the unstable region is therefore unstable for every infinitesimal perturbation in the composition. This form of phase separation is also called spinodal decomposition. In the meta-stable region only a finite perturbation which exceeds a certain critical size (critical nucleus) will result in phase separation, also called nucleation. Perturbations smaller than the critical size will decay. Figure 3.2 shows the solution[1] of equation (3.7) for an unstable (top) and a meta-stable initial
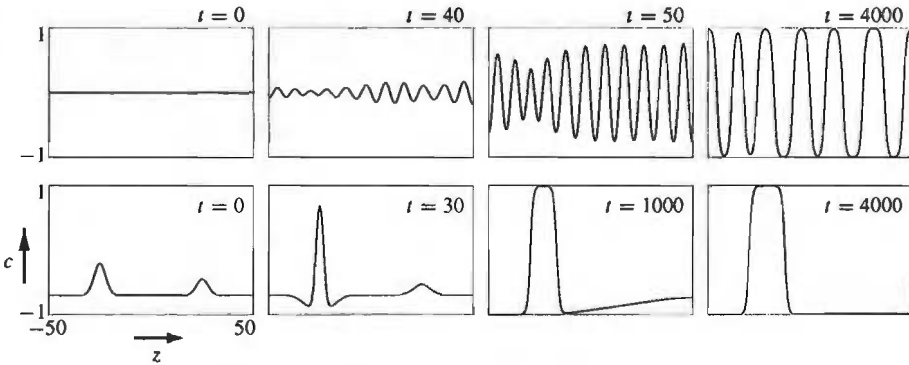

Figure 3.2: *Spinodal decomposition (top) and nucleation (bottom) in a one-dimensional system.*

---

[1] For time discretisation we use the Euler implicit method and for spatial discretisation we use a spectral element method based on Gauss-Lobatto quadrature. Details about the computational method used are given in the next chapter.

condition (bottom). The boundary condition $dc/dz = 0$ and $d\mu/dz = 0$ were used to ensure mass conservation. The top sequence shows spinodal decomposition of an initially unstable mixture ($c = 0$), where a very small random perturbation was used to initiate phase separation. The time sequence at the bottom shows a meta-stable initial state ($c = -0.7$) with a supercritical and sub-critical perturbation. The sub-critical perturbation decays, whereas the supercritical grows. The equilibrium state is reached when the environment is completely depleted. In equilibrium the interface profile is again given by equation (3.6). The one-dimensional nucleation process was studied in detail by Bates and Fife (1993) and Dell'Isola *et al.* (1996).

The assumption of a zero velocity field can not be justified when the densities of the fluids are not the same. The effect of quasi-incompressibility was investigated by Lowengrub and Truskinovsky (1998) by considering phase separation in an inviscid, quasi-incompressible, binary fluid. They found that compressibility has little effect on the interface structure for a spherically symmetric nucleation process in the absence of velocity. In the dynamic case, considering spinodal decomposition in quasi-incompressible binary fluids, they found that diffusion driven flow can occur.

In dimensions greater than one, the local balance equations for mass fraction and momentum are obviously coupled through curvature and interfacial tension. Interfacial tension γ can be defined as the excess tangential stress (Davis and Scriven, 1982). For a planar interface this reads

$$\gamma = \int\limits_{-\infty}^{\infty} \hat{n}\cdot(\tau_r\cdot\hat{n} - \tau_r\cdot\hat{t})\,dz\,, \tag{3.8}$$

where τ_r is the reversible part of the stress tensor and $\hat{n}$ and $\hat{t}$ are the unit vectors normal and tangential to the interface, respectively. Using equation (2.79) with $N = 2$ for τ_r, the interfacial tension can be written as

$$\gamma = \rho\epsilon \int\limits_{-\infty}^{\infty} \left(\frac{dc}{dz}\right)^2 dz\,. \tag{3.9}$$

Using the equilibrium profile (3.6), we obtain

$$\gamma = \frac{2\sqrt{2}}{3}\frac{\rho\epsilon}{\xi}c_B^2\,. \tag{3.10}$$

Neglecting inertia, momentum conservation (2.95) for a density-matched, viscosity-matched binary fluid in the absence of an external force can be written as

$$\nabla g = \nu\nabla^2 v + \mu\nabla c\,. \tag{3.11}$$

Using the dimensionless variables defined above and in addition $v^* = v\xi/D$ and $g^* = g\xi^2/(\epsilon c_B)$, we obtain the following dimensionless momentum equation

$$\nabla g = Ca\nabla^2 v + \mu\nabla c\,. \tag{3.12}$$

The capillary number Ca is defined by

$$Ca = \frac{\nu D}{\epsilon c_B^2} = \frac{2\sqrt{2}}{3}\frac{\eta D}{\gamma \xi} \, , \tag{3.13}$$

where we used equation (3.10).
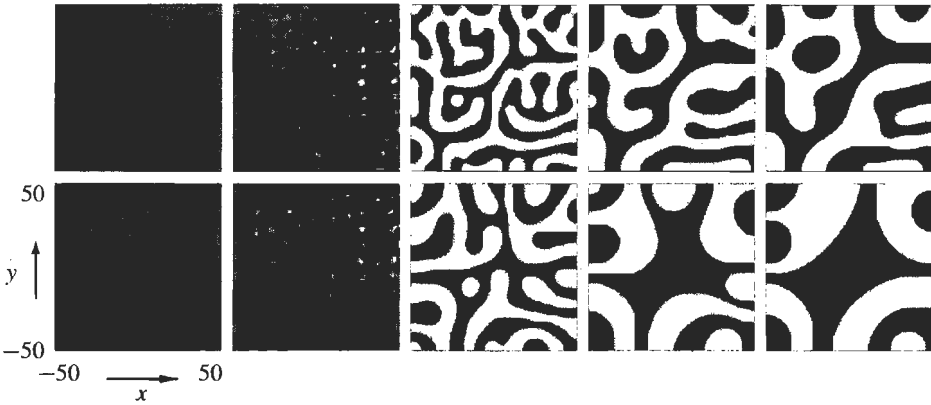
Figure 3.3: *Time sequence ($t = 0, 50, 150, 500, 1000$) of spinodal decomposition in a two-dimensional binary fluid for $Ca = 10^3$ (top) and $Ca = 1$ (bottom).*

Figure 3.3 shows the solution of equation (3.12) and the two-dimensional equivalent of equation (3.7) for an initially unstable solution using $Ca = 10^3$ (top) and $Ca = 1$ (bottom), which are typical values for the capillary number considering that D and ξ have the same order of magnitude. The results show a difference in the coarsening process: for $Ca = 10^3$ the coarsening is slower.

The effect of the viscosity induced coupling between diffusion and motion on the coarsening process for off-critical quenches in binary, isothermal fluids was investigated in detail by Gurtin *et al.* (1996). They found that the hydrodynamic interactions in the system caused flow-induced coalescence of droplets, which results in an enhanced coarsening process. That is, the late-stage coarsening is faster than predicted by the classical, diffusion controlled scaling laws. Jasnow and Viñals (1996) investigated the effect of a temperature gradient on spinodal decomposition in a binary fluid. They concluded that the inclusion of hydro-dynamic coupling washes out the directional coarsening, which arises in the case that the hydrodynamic coupling is not included.

In this section we only considered small scale systems. We used the interfacial thickness, typically $0.1 nm$, as a length scale and the diffusion time, typically $0.1 ns$ as a time scale. For these scales, the computational domain used in figure 3.3 corresponds to a domain which typically measures $10^2 nm^2$. If we want to extend to much larger systems, the real interfacial thickness can not be captured numerically in general. This forces us to use a numerical interfacial thickness which is much larger than the real one. The scaling of such systems needs special attention: we have to make sure that, if we change the interfacial thickness, we are still describing the same system with the same interfacial tension and diffusion. This

issue is briefly discussed in the next section, where we investigate interfacial instabilities. A more detailed discussion of the scaling problem can be found in chapters 5 and 6.

3.3 Interfacial instabilities

Interfacial instabilities are a result of destabilising pressure gradients near a perturbed interface. If we can neglect inertia, the momentum equation (2.95) provides three possible sources for these destabilising pressure gradients: density gradients in an external force field, viscosity gradients in a spatially varying velocity field and interfacial tension gradients. In the first case an interface can become unstable if a more dense fluid is placed on top of a less dense one (Rayleigh-Taylor instability). The second case can lead to instabilities if a less viscous fluid is displacing a more viscous one (viscous fingering). Thirdly, in some cases, local stretching and shrinking of interfaces due to interfacial tension gradients can lead to a destabilising convection (Marangoni instability) in the surrounding liquid. In the next chapter we consider Marangoni instabilities within the framework of thermo-capillary flow.

In this section we briefly discuss Rayleigh-Taylor instabilities and viscous fingering in a Hele-Shaw cell, which consists of two closely spaced parallel plates (Saffman and Taylor, 1958). Consider two, isothermal, non-wetting fluids in a Hele-Shaw cell as depicted in figure 3.4. One fluid is displacing the other one with a velocity v_I. The cell is tilted off axis at an angle θ (see figure 3.4), such that the external force which acts on the fluid inside the cell equals $f_g \sin \theta$. The plates are assumed to be perfectly smooth such that the contact lines can
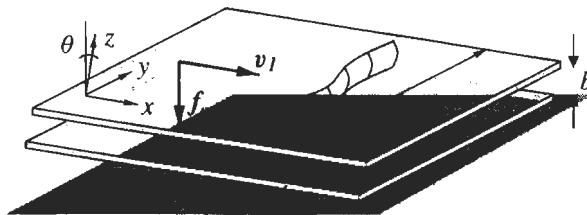
Figure 3.4: Schematic picture of a displacement flow in a Hele-Shaw cell.

move freely. We assume that the plate spacing b and the Reynolds number $Re = Vb/\nu$ are small, such that inertial terms in the momentum equation can be neglected and the bulk flow between the plates can be assumed to be a Poiseuille flow. Formally, this approximation is not valid for the interface: the moving interface problem involves a complicated small-scale flow near the contact lines (Seppecher, 1996; Jacqmin, 1996)[2]. The assumption of a Poiseuille flow automatically implies that $\partial p / \partial z = 0$. In addition, we assume that the mass fraction c is independent of z. Using these assumptions we can average the governing three dimensional equations, (2.93) to (2.95), over the gap. This yields the following set of two-dimensional

---

[2] The diffuse-interface results of Jacqmin (1996) match the experimental results on moving contact lines of Dussan V and Davis (1974).

equations

$$\frac{d\rho}{dt} = -\rho \nabla \cdot \boldsymbol{v} \, , \tag{3.14}$$

$$\rho \frac{dc}{dt} = \frac{\Lambda}{T} \nabla^2 \mu^{\bullet} \quad \text{with} \quad \mu^{\bullet} = \frac{\partial f}{\partial c} - \frac{1}{\rho} \nabla \cdot (\rho \frac{\partial f}{\partial \nabla c}) + \kappa p \, , \tag{3.15}$$

$$\rho \nabla g = \eta \nabla^2 \boldsymbol{v} - \frac{12\eta}{b^2} \boldsymbol{v} - \frac{2}{3} \eta \nabla \cdot \boldsymbol{v} \boldsymbol{I} + \rho \mu^{\bullet} \nabla c + \rho f_g \sin \theta \, , \tag{3.16}$$

where $\boldsymbol{v} = (v_x, v_y)$ is velocity averaged over the gap and the density ρ is given by the simple mixture relation: $2/\rho = (1-c)/\varrho_2 + (1+c)/\varrho_1$. The second term on the right hand side of equation (3.16) is the Darcy term, which takes into account the friction force of the flow due to the plates. In most systems with a small plate spacing, the Stokes term (the first term on the right hand side of equation (3.16)) can be neglected[3]. This set of equations can be further simplified using a Boussinesq approximation (Lowengrub *et al.*, 1998): the density difference is small, such that it can be neglected in all terms except the gravitational term. This way, we obtain

$$\nabla \cdot \boldsymbol{v} = 0 \, , \tag{3.17}$$

$$\frac{dc}{dt} = \frac{\Lambda}{\varrho_1 T} \nabla^2 \mu \quad \text{with} \quad \mu = \beta c^3 - \alpha c - \epsilon \nabla^2 c \, , \tag{3.18}$$

$$\nabla g = \mu \nabla c - \frac{12\eta}{\varrho_1 b^2} \boldsymbol{v} + \frac{\rho}{\varrho_1} f_g \sin \theta \, , \tag{3.19}$$

where, as in section 3.2, we used the Ginzburg-Landau approximation for f. By using the Boussinesq approximation we avoid the effects of quasi-incompressibility. For this two-dimensional problem it is convenient to rewrite equation (3.19) in terms of the stream function ψ, which is defined by $\boldsymbol{v} = (\partial \psi / \partial y, -\partial \psi / \partial x)$. The local balance equation for ψ is obtained by taking the curl ($\nabla \times$) of the momentum equation. This yields

$$-\frac{12}{\varrho_1 b^2} \nabla \cdot (\eta \nabla \psi) = \nabla \times \mu \nabla c + \nabla \times \zeta c f_g \sin \theta \, , \tag{3.20}$$

where we have approximated the density as $\rho/\varrho_1 = 1 + \zeta c$ with $\zeta = \frac{1}{2}(\varrho_1 - \varrho_2)/\varrho_1$.

To write the governing equations in a non-dimensional form we use the following dimensionless variables: $c^* = c/c_B$, $\mu^* = \mu \xi^2/(\epsilon c_B)$, $\nabla^* = L\nabla$, $\boldsymbol{v}^* = \boldsymbol{v}/V$ and $t^* = tV/L$, where V is the characteristic velocity and L is the lateral size of the cell. Omitting the asterisk notation, the dimensionless equations now read

$$\frac{dc}{dt} = \frac{1}{Pe} \nabla^2 \mu \quad \text{with} \quad \mu = c^3 - c - C^2 \nabla^2 c \, , \tag{3.21}$$

$$-k^2 Ca \nabla \cdot (\eta \nabla \psi) = \frac{1}{C} \nabla \times \mu \nabla c + Bo \nabla \times c f_g \, , \tag{3.22}$$

---

[3] In the next chapter, where we consider thermo-capillary flow, it can not always be neglected, because velocity gradients parallel to the plates can be large in that case.

where $k^2 = 12L^2/b^2$ is the dimensionless permeability and the Peclet, Cahn, capillary and Bond number are given by

$$Pe = \frac{LV}{D}, \quad C = \frac{\xi}{L}, \quad Ca = \frac{2\sqrt{2}}{3}\frac{\eta_1 V}{\gamma} \quad \text{and} \quad Bo = \frac{2\sqrt{2}}{3}\frac{\varrho_1 \zeta |f_g| \sin\theta L^2}{\gamma}, \tag{3.23}$$

respectively.

First, we consider the Rayleigh-Taylor instability: the viscosity is assumed to be constant and the injection velocity v_I equals zero. Figure 3.5 shows how interfacial tension affects the stability: in the picture on the left hand side interfacial tension is low compared to the gravitational force and on the right hand side it is high. More precise: on the left we used
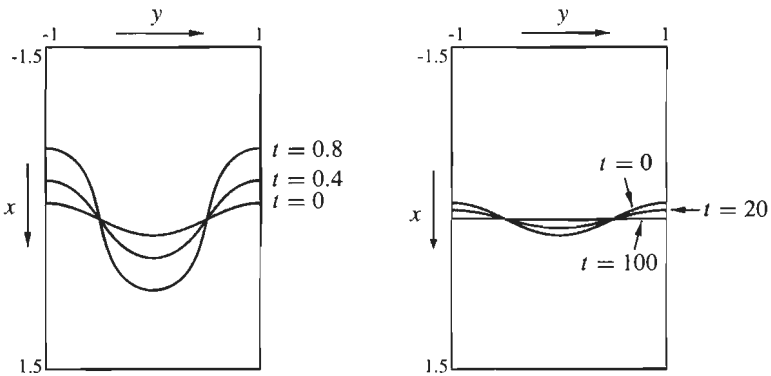
Figure 3.5: *Time evolution of an unstably stratified binary fluid, where the capillary force is small compared to gravitational force on the left and large on the right.*

$Bo = k^2$ and on the right $Bo = k^{-2}$. Furthermore, we used $Ca = 1$, $Pe = 10^3$, $k = 10\sqrt{12}$, $C = 0.05$ and domain size 2×3 in both cases. Starting with the same initial perturbation at $t = 0$ the system with low interfacial tension becomes unstable, whereas it is stable when the interfacial tension is high.

As stated in the previous section, the choice for ξ in large scale systems is somewhat arbitrary, since it is no longer directly coupled to the real value of the interfacial thickness. We assume that the interfacial tension keeps its value if we change ξ, that is the capillary number and the Bond number are independent of ξ. The Cahn number and the Peclet number, however, still depend on ξ. In figure 3.6 we consider the same situation as in the left hand side picture of figure 3.5, but we vary the Cahn number (left) and the Peclet number (right) to see how this affects the results. On the left, the interface at $t = 0.8$ is shown for various values of the Cahn number and on the right, for various values of the Peclet number. The results show that increasing the Cahn number and decreasing the Peclet number has a stabilising effect. In both cases we find convergence, which might indicate there is a sharp-interface limit. However, the scaling concerning the sharp-interface limit is more complicated than just taking $C \rightarrow 0$ and $Pe \rightarrow \infty$. Equation (3.10) shows that to obtain a finite value for γ in the sharp-interface limit, ϵc_B^2 has to be proportional to ξ. This will also affect the scaling for the Peclet number. A detailed discussion of this issue is postponed to chapter 5.
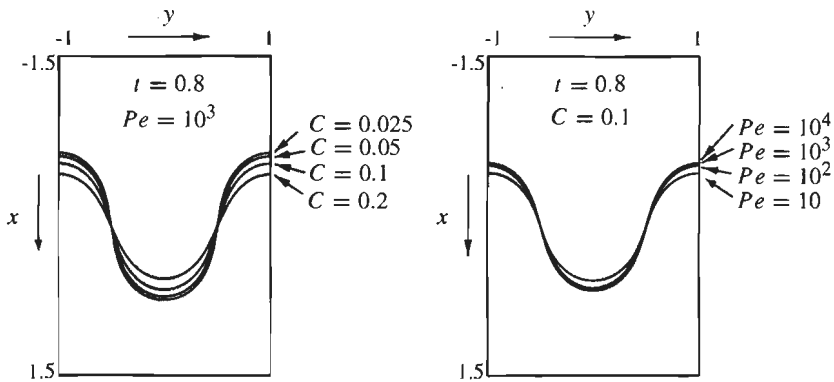
Figure 3.6: *Interface profile for the unstable situation in figure 3.5 at t = 0.8 for various values of the Cahn number C (left) and the Peclet number Pe (right).*

Finally, we consider viscous fingering: one of the fluids is displacing the more viscous one with a velocity v_I. The viscosity is chosen to be a linear function of c, such that the viscosity ratio of the two fluids equals 10. Figure 3.7 shows the time development of an initially planar
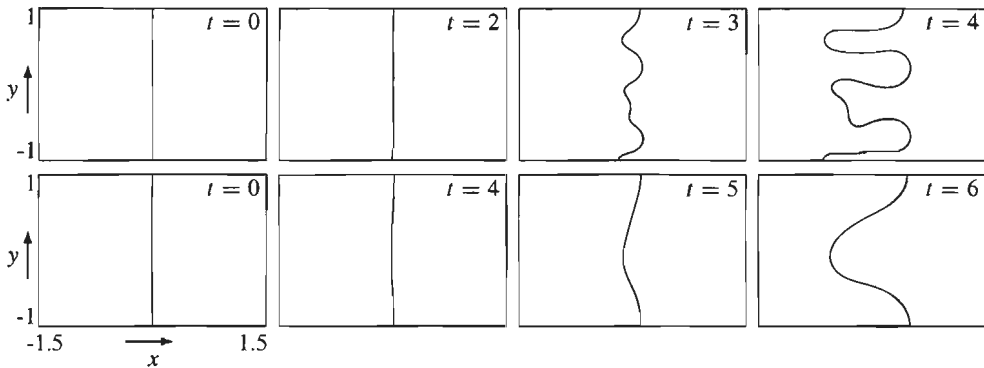
Figure 3.7: *Viscous fingering for Ca = 10 (top) and Ca = 0.1 (bottom).*

interface with a small random perturbation, in a reference frame moving with the injection velocity v_I, for two values of the capillary number: $Ca = 10$ (top) and $Ca = 0.1$ (bottom). Moreover, we used $C = 0.1$, $Bo = 0$ and $Pe = 500$ in both cases. Again, the results show the stabilising effect of interfacial tension: for $Ca = 0.1$ the growth rate of the instability is smaller and a larger wavelength is picked up, which is in qualitative agreement with a linear stability analysis (Bensimon *et al.*, 1986). The dependence of this system on the Peclet and the Cahn number is similar to the dependence for the Rayleigh-Taylor instability: for smaller Cahn numbers and for larger Peclet numbers a slightly larger growth rate is observed.

In this section, we only considered viscous fingering and Rayleigh-Taylor instabilities separately. If both are included, there can be competing effects: for instance when the less

viscous fluid has got a smaller density. In miscible systems, these competing effects were investigated by Manickam and Homsy (1995). Furthermore, they also considered nonlinear viscosity profiles, which can lead to reverse fingering. Immiscible displacement flows were considered in detail by Bensimon *et al.* (1986). In their review paper they also consider the zero surface tension limit, in which tip splitting can result in fractal interface structures.

3.4 Conclusions

In this chapter we investigated phase separation and interfacial instabilities in a Hele-Shaw cell. Phase separation was considered in small-scale systems in which the physical value of the interfacial thickness can be captured numerically. Interfacial instabilities, discussed in section 3.3, normally have a length scale which is much larger than the physical value of the interfacial thickness. In this case, the interfacial thickness can not be captured numerically and has to be replaced by a numerically acceptable one. In this case, the scaling needs special attention.

Convergence was observed for the Rayleigh-Taylor instability for $C \rightarrow 0$ and $Pe \rightarrow \infty$. This might be a first indication that the diffuse-interface approach can also be used to model large-scale systems and that it might be possible to bridge the gap between small-scale and large-scale systems in this way.

However, in section 3.3 it was also argued that the scaling is more complicated than just taking $C \rightarrow 0$ and $Pe \rightarrow \infty$. In the next two chapters, the scaling problem will be investigated in more detail.

Chapter 4

THERMO-CAPILLARY FLOW AND
INSTABILITIES IN A HELE-SHAW CELL

This chapter is partly after:
'Diffuse-interface modelling of thermo-capillary instabilities in a Hele-Shaw cell'.
M. Verschueren, F.N. van de Vosse and H.E.H Meijer.
J. Fluid Mech.
(submitted)

4.1   Introduction

An imposed temperature gradient along an interface between immiscible fluids can induce a flow if the interfacial tension depends on temperature. This phenomenon is called thermo-capillary or Marangoni flow (Davis, 1987) and is often encountered in industrial processing (Edwards *et al.*, 1991). In industrial processes thermo-capillary flow is often accompanied by other phenomena which involve topological changes in interfaces, such as coalescence, break-up and phase separation (Kuhlmann, 1999). In general, interfacial tension depends not only on temperature. It can also depend strongly on the concentration of a foreign component at the interface. This situation can lead to spontaneous interfacial activity, called 'interfacial turbulence' by Sternling and Scriven (1959). In some cases the interfacial deformation is so strong that droplets are pinching off (Sherwood and Wei, 1957). The goal of the present chapter is to find a physical model and an appropriate numerical implementation which can describe thermo-capillary flow allowing for topological changes.

In the classical approach to multi-component flow, an interface is assumed to be sharp and appropriate boundary conditions are applied to connect the various components. Solving the equations of fluid dynamics therefore involves solving a moving boundary problem. The most 'natural' numerical technique in this case is the tracking method (Hyman, 1984; Unverdi and Tryggvason, 1992): the discretisation is such that grid points follow the interface. In case of topological changes the tracking method is inconvenient, since complicated re-meshing is necessary. To overcome this problem, Brackbill *et al.* (1991) developed a continuum surface force (CSF) method in which the sharp interface is replaced by an artificial, continuous colour function. This colour function is used to determine the position and the geometry of the

interface. Interfacial tension can now be included in the equation of motion as a body force. A direct application of boundary conditions is no longer required in this case and a fixed grid numerical method can be used, which is convenient in case of topological changes. The disadvantage of the CSF method is that the colour function is an arbitrary function without a physical meaning. It can be shown that numerical results are sensitive to the choice of this colour function (Lowengrub and Truskinovsky, 1998).

In diffuse-interface theories, which go back to the ideas of van der Waals (1979), the interface also has a non-zero thickness, but it is no longer arbitrary. It is determined by the molecular force balance at the interface and its value is closely related to the finite range of molecular interactions (Rowlinson and Widom, 1989). Thermodynamically, the finite inter-action range is represented by a nonlocal effect in the free energy: the local free energy density not only depends on the local composition, but also on the composition of the immediate environment (Davis and Scriven, 1982). Cahn and Hilliard (1958) used a Taylor expansion of the free energy density about the homogeneous system. In this way, the nonlocal effect is represented by a dependence on local composition gradients rather than non-local composition. Non-classical expressions for the chemical potential and the stress tensor can then be derived in differential form, which allows a direct coupling with the equations of fluid dynamics.

The diffuse-interface approach has been used to study a wide range phenomena such as nucleation, spinodal decomposition, capillary waves, instabilities, mixing and moving contact lines. A review on recent developments in diffuse-interface modelling is given by Anderson *et al.* (1998). Antanovskii (1995) studied thermo-capillary flow in the one-dimensional case using the diffuse-interface approach and Jasnow and Viñals (1996) studied thermo-capillary motion of small droplets. Jasnow and Viñals also derived the sharp-interface expression for interfacial tension (gradients) from their diffuse-interface capillary term in the momentum equation, but they only show results for very small droplets. In this chapter we focus on the question whether the diffuse-interface model can be applied to droplets with radii much larger than the physical interfacial thickness.

We study thermo-capillary motion in a Hele-Shaw cell. The results for pinned planar and circular interfaces are directly compared to the analytical results of Boos and Thess (1997). The dependence on the interfacial thickness is investigated, considering the sharp interface limit. Finally, we study thermo-capillary instabilities caused by a temperature gradient perpendicular to the interface. In section 2 we define the system to be investigated. In section 3 the diffuse-interface theory is presented and non-classical expressions for the diffusion flux and the reversible part of the stress tensor are derived, following the principles of classical irreversible thermodynamics (de Groot and Mazur, 1984). Section 4 is devoted to the numerical implementation of the governing equations, focusing on the Gauss-Lobatto spectral element discretisation. Results are presented and discussed in sections 5 and 6. Finally, section 7 contains some conclusions.

4.2   System definition

We consider two immiscible, incompressible, non-wetting fluids in a Hele-Shaw cell, which consists of two, closely spaced parallel plates (see figure 4.1). We assume that the two fluids have equal density ρ and dynamic viscosity η. Along both plates, which are assumed to have
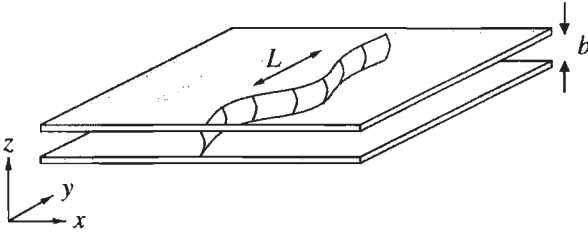
Figure 4.1: *Schematic picture of a Hele-Shaw geometry, where b is the distance between the plates and L is the structure size of the interface.*

a large thermal conductivity, a temperature gradient of the following form is imposed

$$T = T_o + A\hat{e}_T \cdot r \, , \tag{4.1}$$

where A is a constant, $\hat{e}_T$ is the unit vector in the direction of the temperature gradient and $r = (x, y)$ is the spatial coordinate parallel to the plates. Interfacial tension γ is assumed to be a function of the temperature. For most fluids interfacial tension decreases with an increasing temperature. We assume that the thermal Peclet number is small, that is $Pe_T = Vb/\lambda \ll 1$, where V is the thermo-capillary velocity scale and λ is the heat diffusivity of the fluid. In this case the effect of fluid motion on the temperature field can be neglected[1], which means that the temperature of the fluid between the plates is also given by equation (4.1).

For small Reynolds numbers $Re = Vb/\nu$, with $\nu = \eta/\rho$ is the kinematic viscosity, fluid flow is governed by the Stokes equations, which read in dimensionless form

$$\nabla^{(3)} \cdot v^{(3)} = 0 \, , \tag{4.2}$$

$$\nabla^{(3)} \cdot \tau^{(3)} = 0 \, , \tag{4.3}$$

where $\nabla^{(3)} = (\partial/\partial x, \partial/\partial y, \partial/\partial z)$, $v^{(3)}$ is the three dimensional velocity and $\tau^{(3)} = -p^{(3)}\mathbf{I} + \nabla^{(3)}v + \nabla^{(3)}v^\mathsf{T}$ is the stress tensor, with $p^{(3)}$ the pressure $\mathbf{I}$ the unit dyad. The kinematic and the stress boundary condition are

$$[\![v^{(3)}]\!] = 0 \, , \tag{4.4}$$

$$[\![\tau^{(3)} \cdot \hat{n}]\!] = \frac{1}{Ca}(\gamma\hat{n}\nabla_s^{(3)} \cdot \hat{n} - \nabla_s^{(3)}\gamma) \, , \tag{4.5}$$

respectively, where $Ca = \nu V/\gamma_o$ is the capillary number, $\hat{n}$ is the unit vector normal to the interface and $\nabla_s^{(3)} = (\mathbf{I} - \hat{n}\hat{n}) \cdot \nabla^{(3)}$ denotes the interface gradient.

For non-wetting fluids in a Hele-Shaw geometry with small plate spacing b the bulk flow is a Poiseuille flow. In this case the three-dimensional governing equations can be averaged over the gap. This yields the following set of two-dimensional governing equations

$$\nabla \cdot v = 0 \, , \tag{4.6}$$

$$\nabla p = \nabla^2 v - k^2 v \, , \tag{4.7}$$

---

[1] It can be shown that, even if the heat diffusivity of the fluid is zero, the deviation from the plate temperature T is still small as long as the temperature gradient A and the plate spacing b are small (Boos and Thess, 1997).

where $\nabla = (\partial/\partial x, \partial/\partial y)$, $v = (v_x, v_y)$ is the velocity averaged over the gap and $k = 12L^2/b^2$ is the dimensionless permeability of the cell. Equation (4.7) is the two-dimensional Stokes equation with an additional Darcy term, which takes into account the friction force of the flow due to the plates. The Darcy term is normally assumed to be much larger than the Stokes term. However, this approximation is only valid if the structure size L is much larger than the plate spacing and if the velocity gradients parallel to the plates are small compared to velocity gradients perpendicular to the plates. In case of thermo-capillary flow, velocity gradients parallel to the plates can be large in a small region near the interface.

We assume that Stokes-Darcy equation (4.7) also applies to the interface and we will not consider any small-scale flow phenomena in the vicinity of the contact lines[2]. The contact lines are assumed to be either pinned or freely movable. In case of pinned contact lines the normal component of the kinematic boundary condition is $v \cdot \hat{n} = 0$.

The necessity to apply boundary conditions (4.4) and (4.5) is very inconvenient in case of large interfacial deformations or topological changes in the interface. Furthermore, the physical mechanism controlling topological changes is missing. In the next section we present the diffuse-interface theory, which includes the physical mechanism by considering non-local effects in the free energy of the system. All properties vary continuously across the interface, which allows us to include interfacial tension as a locally acting body force.

4.3   Diffuse-interface theory

Diffuse-interface theories are based on non-local effects in the free energy of the system. As stated in the first section, these non-local effects can be represented by a dependence on local composition gradients. Therefore we start with the assumption that the specific internal energy u depends not only on the entropy s and the mass fraction of one of the components c, but also on the gradient of c. That is $u = u(s, c, \nabla c)$. Besides the continuity equation and the Stokes equation, we now also need the local balance equations[3] for c, u and s

$$\rho \frac{dc}{dt} = -\nabla \cdot j \, , \tag{4.8}$$

$$\rho \frac{du}{dt} = \tau : \nabla v - \nabla \cdot q \, , \tag{4.9}$$

$$\rho \frac{ds}{dt} = -\nabla \cdot j_s + \sigma \, , \tag{4.10}$$

where j is the diffusion flux, q is the energy flux, j_s is the entropy flux and σ is the entropy production. The second law of thermodynamics states that we must have $\sigma \geq 0$, where the equal sign applies for systems in equilibrium or reversible changes. In the diffuse-interface approach the stress tensor τ also includes interfacial tension and is, therefore, no longer defined by the classical relation given in the section 2. One expects an additional reversible part, depending on ∇c, which includes interfacial tension as a body force. In a similar way, the diffusion flux j and the energy flux q also depend on ∇c.

To find relations for j, τ and q, we follow the principles of classical irreversible thermodynamics (de Groot and Mazur, 1984): the fluxes are assumed to be linear functions of the

---

[2] Jacqmin (1996) studied fluid motion near a moving contact line, using the diffuse-interface approach.

[3] In this section we will omit the superscript [(3)] for three dimensional systems

thermodynamic forces appearing in the entropy production σ. A more explicit expression for σ can be found by considering the Gibbs relation, which is given by the total differential of u. Assuming local equilibrium for a volume element moving with the flow (de Groot and Mazur, 1984), the Gibbs relation reads

$$\frac{du}{dt} = \left.\frac{\partial u}{\partial s}\right|_{c,\nabla c} \frac{ds}{dt} + \left.\frac{\partial u}{\partial c}\right|_{s,\nabla c} \frac{dc}{dt} + \left.\frac{\partial u}{\partial \nabla c}\right|_{s,c} \cdot \frac{d\nabla c}{dt} . \tag{4.11}$$

In the sequel we omit the subscripts denoting the variables which are kept constant. The local balance equation for ∇c can be found by considering the gradient of equation (4.8). After some manipulations we find

$$\frac{d\nabla c}{dt} = -\nabla v \cdot \nabla c - \nabla(\frac{1}{\rho}\nabla \cdot j) . \tag{4.12}$$

Combining equations (4.8) to (4.12) we obtain the following relation for the entropy production[4]

$$\sigma = \frac{1}{T}(\tau - \tilde{\tau}) : \nabla_d v + (q - \tilde{q})\nabla\frac{1}{T} - j \cdot \nabla\frac{\mu}{T} , \tag{4.13}$$

where $\nabla_d v$ is the deviatoric part of ∇v and

$$\tilde{\tau} = -\rho\frac{\partial u}{\partial \nabla c}\nabla c , \tag{4.14}$$

$$\tilde{q} = \rho\frac{\partial u}{\partial \nabla c}\nabla \cdot j \quad \text{and} \tag{4.15}$$

$$\mu = \frac{\partial u}{\partial c} - \nabla \cdot \frac{\partial u}{\partial \nabla c} \tag{4.16}$$

are the reversible part of the stress tensor, the energy flux due to mass diffusion and the generalised chemical potential, respectively. The entropy production has a simple structure: it is the sum of the products of the thermodynamic fluxes and forces. In equilibrium both fluxes and forces vanish. Consequently, the equilibrium part of the diffusion and the energy flux are equal to zero and the reversible part of the stress tensor can be written as $\tau_r = -p\mathbf{l} + \tilde{\tau}$, where p is an arbitrary pressure field.

The dissipative parts of fluxes, the viscous stress tensor $\tau_v = \tau - \tau_r$, the energy flux q and the diffusion flux j, are assumed to be linear functions of the thermodynamic forces. Keeping in mind that fluxes and forces of different tensorial character do not couple, we obtain

$$\tau_v = \frac{\Lambda_v}{2T}(\nabla v + \nabla v^{\mathsf{T}}) , \tag{4.17}$$

$$q = -\Lambda_{qq}\nabla\frac{1}{T} - \Lambda_{qj}\nabla\frac{\mu}{T} , \tag{4.18}$$

$$j = -\Lambda_{jq}\nabla\frac{1}{T} - \Lambda_{jj}\nabla\frac{\mu}{T} , \tag{4.19}$$

---

[4] For more details see chapter 2.

where we have assumed that the viscous stress tensor is symmetric. The Λ's are the phenomenological coefficients. The coefficient $\Lambda_v/2T$ can be identified as the shear stress η, Λ_{qq}/T^2 is the heat conductivity and Λ_{jj} is the mobility parameter. Equations (4.18) and (4.19) also include the cross-effects, the Soret and the Dufour effect (Bird *et al.*, 1960), which will be neglected in the sequel.

In this chapter we are only concerned with small linear temperature gradients which do not change in time. In this case the governing equations are given by

$$\nabla \cdot v = 0 \, , \tag{4.20}$$

$$\rho \frac{dc}{dt} = \frac{\Lambda_{jj}}{T_o} \nabla^2 \mu \, , \tag{4.21}$$

$$\nabla \cdot (\tau_r + \tau_v) = 0 \, , \tag{4.22}$$

where we have assumed that Λ_{jj} is constant. To complete this set of equations we need an equation of state for the inhomogeneous system. Using a Taylor expansion about the homogeneous system, Cahn and Hilliard (1958) derived the following form for the specific Helmholtz free energy

$$f(T, c, \nabla c) = f_h(T, c) + \frac{1}{2} \epsilon |\nabla c|^2 \, , \tag{4.23}$$

where ϵ is the gradient energy parameter, which is assumed to be constant. Using an additional Taylor expansion of f_h about the critical temperature T_c and the critical composition c_c yields the Ginzburg-Landau form (Gunton *et al.*, 1983)

$$f(T, \tilde{c}, \nabla \tilde{c}) = \frac{1}{4} \beta \tilde{c}^4 - \frac{1}{2} \alpha (T_c - T) \tilde{c}^2 + \frac{1}{2} \epsilon |\nabla \tilde{c}|^2 \, , \tag{4.24}$$

where $\tilde{c} = c - c_c$. The parameters α and β are both positive constants. Using the thermodynamic relations $\partial u/\partial c|_{s,\nabla c} = \partial f/\partial c|_{T,\nabla c}$ and $\partial u/\partial \nabla c|_{s,c} = \partial f/\partial \nabla c|_{T,c}$ the chemical potential (4.16) can be written as

$$\mu = \beta c^3 - \alpha (T_c - T) c - \epsilon \nabla^2 c \, , \tag{4.25}$$

where we have omitted the tilde notation. In equilibrium μ equals zero. Besides the spatially uniform (bulk) solutions $c = \pm c_B$, with $c_B = \sqrt{\alpha(T_c - T)/\beta}$, there is another possible solution, which represents the interface profile. For a planar interface, with z the direction normal to the interface, this solution is given by

$$c = c_B \tanh \frac{z}{\sqrt{2}\xi} \quad \text{with} \ \xi = \sqrt{\frac{\epsilon}{\alpha(T_c - T)}} \, , \tag{4.26}$$

where ξ is the interfacial thickness.

Interfacial tension γ is determined by the choice of the equation of state. It can be defined as the excess tangential stress:

$$\gamma = \int_{-\infty}^{\infty} \hat{n} \cdot (\tau_r \cdot \hat{n} - \tau_r \cdot \hat{t}) dz = \rho \epsilon \int_{-\infty}^{\infty} (dc/dz)^2 dz \, . \tag{4.27}$$

Using equation (4.26) we obtain

$$\gamma = \frac{2\sqrt{2}}{3}\frac{\rho\sqrt{\epsilon}}{\beta}[\alpha(T_c - T)]^{\frac{3}{2}} . \tag{4.28}$$

In the momentum equation interfacial tension is included in $\nabla\cdot\boldsymbol{\tau}_r$. For small temperature gradients $\nabla\cdot\boldsymbol{\tau}_r$ can be rewritten as $\nabla\cdot\boldsymbol{\tau}_r = -\nabla\rho g + \rho\mu\nabla c$, where $g = f + p/\rho$ is the specific Gibbs free energy. The momentum equation can then be written as[5]

$$\nabla g = \nu(\nabla^2\boldsymbol{v} - k^2\boldsymbol{v}) + \mu\nabla c , \tag{4.29}$$

where we used the Stokes-Darcy approximation for the viscous part. Computationally, it is convenient to rewrite the momentum equation in terms of the stream function ψ, which is defined by $\boldsymbol{v} = (\partial\psi/\partial y, -\partial\psi/\partial x)$. This way mass conservation is automatically satisfied. The equation for ψ is found by taking the curl of equation (4.29). This yields

$$\nu\nabla^2(\nabla^2\psi - k^2\psi) = \nabla\times\mu\nabla c , \tag{4.30}$$

where $\nabla\times$ denotes the curl.

To scale the governing equations we use the following dimensionless variables: $c^* = c/c_{Bo}$, $\boldsymbol{r}^* = \boldsymbol{r}/L$, $\boldsymbol{v}^* = \boldsymbol{v}/V$, $\mu^* = \mu\xi_o^2/(\epsilon c_{Bo})$, $t^* = tV/L$, $T^* = T/T_o$ and $\psi^* = \psi/(LV)$, where $\xi_o = \xi(T_o)$ and $c_{Bo} = c_B(T_o)$. Omitting the asterisk notation we obtain the following dimensionless governing equations

$$\frac{dc}{dt} = \frac{1}{Pe}\nabla^2\mu \quad \text{with } \mu = c^3 - (1 - \zeta\hat{\boldsymbol{e}}_T\cdot\boldsymbol{r})c - C^2\nabla^2 c , \tag{4.31}$$

$$\nabla^2(\nabla^2\psi - k^2\psi) = \frac{1}{Ca}\frac{1}{C}\nabla\times\mu\nabla c , \tag{4.32}$$

where the Peclet number Pe, the temperature parameter ζ, the Capillary number Ca and the Cahn number C are given by

$$Pe = \frac{\rho T_o\xi_o^2 LV}{\Lambda_{jj}\epsilon} \quad \zeta = \frac{AL}{T_c - T_o} \quad Ca = \frac{\xi_o\nu V}{\epsilon c_{Bo}^2} \quad \text{and} \quad C = \frac{\xi_o}{L} , \tag{4.33}$$

respectively.

Analytical solutions can only be obtained in some special cases. In general a numerical implementation is needed.

4.4 Computational methods

To discretise the governing equations we use a spectral element method (Timmermans *et al.*, 1994). The computational domain Ω is divided into N_{el} non-overlapping sub-domains Ω_e and a spectral approximation is applied on each element. The basis functions ϕ, which are used for the spatial discretisation, are high-order Lagrange interpolation polynomials through the Gauss-Lobatto integration points defined per element.

---

[5] from now the equations are two dimensional

The momentum equation (4.29) is a fourth order differential equation in ψ. Since the basis functions ϕ are elements of H^1, that is $H^1(\Omega) = \{\phi \mid \phi \in L^2(\Omega), \nabla\phi \in L^2(\Omega) \times L^2(\Omega)\}$, we split up the momentum equation into two second order differential equations

$$\nabla^2 Q = h \, , \tag{4.34}$$

$$\nabla^2 \psi - k^2 \psi = Q \, , \tag{4.35}$$

where $h = Ca^{-1}C^{-1}\nabla \times \mu\nabla c$. The boundary conditions for Q and ψ are either homogeneous Neumann or Dirichlet. The Galerkin weighted residual representation of the differential equations is

$$(\nabla^2 Q, w)_\Omega = (h, w)_\Omega \, , \tag{4.36}$$

$$(\nabla^2 \psi, w)_\Omega - k^2(\psi, w)_\Omega = (Q, w)_\Omega \, , \tag{4.37}$$

where the inner product $(a, w)_\Omega = \int_\Omega a w d^2 r$ and w is the standard Galerkin test function. Partial integration of the integrals on the left hand side yields weak or variational form

$$- (\nabla Q, \nabla w)_\Omega = (h, w)_\Omega \, , \tag{4.38}$$

$$- (\nabla \psi, \nabla w)_\Omega - k^2(\psi, w)_\Omega = (Q, w)_\Omega \, , \tag{4.39}$$

where the boundary integrals vanished because of the homogeneous boundary conditions. The next step is to decompose the total domain Ω in N_{el} non-overlapping sub-domains Ω_e and apply the spectral discretisation on each element.

$$Q^e = \sum_{l,m=1}^{N} Q^e_{lm} \tilde{\phi}^e_{lm} \, , \tag{4.40}$$

where $\tilde{\phi}_{lm}$ is the two-dimensional Lagrange interpolation function through the Legendre-Gauss-Lobatto integration points $(l, m = 1 \ldots N)$, which is the tensor product of the one-dimensional interpolation functions : $\tilde{\phi}_{lm} = \phi_l \phi_m$. Using similar discretisations for ψ, w and f and assembling the elements we obtain the following discrete set of equations

$$\mathbf{S}Q = \mathbf{M}h \, , \tag{4.41}$$

$$\mathbf{S}\psi - k^2\mathbf{M}\psi = \mathbf{M}Q \, , \tag{4.42}$$

where $\mathbf{S}$ is the diffusion matrix, $\mathbf{M}$ is the mass matrix and Q, h and ψ are the discrete vector representations of Q, h and ψ, respectively.

The composition equation and the equation for the chemical potential is also a set of two second order differential equations, which we will solve in a coupled way. Besides spatial discretisation we now also need temporal discretisation. Using the Euler implicit method for time discretisation and the same spatial discretisation as for the momentum equation we obtain

$$\begin{bmatrix} \mathbf{M} - \Delta t \mathbf{N}^n & \dfrac{\Delta t}{Pe}\mathbf{S} \\[2ex] [1 - \zeta \hat{e}_T \cdot r - (c_i^{n+1})^2]\mathbf{M} - C^2\mathbf{S} & \mathbf{M} \end{bmatrix} \begin{bmatrix} c_{i+1}^{n+1} \\[2ex] \mu_{i+1}^{n+1} \end{bmatrix} = \begin{bmatrix} \mathbf{M}c_0^n \\[2ex] 0 \end{bmatrix} \, , \tag{4.43}$$

where $\mathbf{M}$ is the mass matrix, $\mathbf{N}$ is the convection matrix with $v = (\partial \psi / \partial y, -\partial \psi / \partial x)$ and $\mathbf{S}$ is the diffusion matrix. Superscript n denotes time t and $n + 1$ denotes $t + \Delta t$. A Picard iteration is used to deal with the nonlinear term (subscript $i = 1 \ldots I$): the iteration starts using $c_1^{n+1} = c_0^n$ and as a stopping criterion we use max $|c_{I+1}^{n+1} - c_1^{n+1}| < 10^{-4}$. After convergence, μ_{I+1}^{n+1} and c_{I+1}^{n+1} are used to compute a new h and we can move to the next time step.

4.5 Classical vs. diffuse-interface results

In this section we compare our computational, diffuse-interface results for thermo-capillary flow with classical, analytical results of Boos and Thess (1997) for pinned planar and circular interfaces. We investigate how the results depend on the Cahn number C.

To be able to make a direct comparison with the classical results we have to make sure that we use the same assumptions and the same scaling. In their paper Boos and Thess assumed that γ is a linear function of temperature. That is

$$\gamma = \gamma_o - B(T - T_o) , \tag{4.44}$$

where B is a positive constant. In our case, interfacial tension is given by equation (4.28), which is nonlinear in T. However, for small values of ζ, defined in (4.33), we can approximate γ as

$$\gamma = \frac{2\sqrt{2}}{3} \frac{\rho \epsilon}{\xi_o} c_{Bo}^2 (1 - \frac{3}{2} \zeta \hat{e}_T \cdot r^*) . \tag{4.45}$$

This way we find

$$B = \frac{d\gamma}{dT} = \frac{1}{AL} \frac{d\gamma}{d\hat{e}_T \cdot r^*} = \sqrt{2} \frac{\rho \epsilon}{\xi_o} c_{Bo}^2 \frac{1}{T_c - T_o} . \tag{4.46}$$

Boos and Thess used $V = \frac{1}{2} ABL/\eta$ as the velocity scale. In our case this yields

$$Ca = \frac{1}{2} \sqrt{2} \zeta . \tag{4.47}$$

For small temperature gradients we can also approximate the composition profile c by the equilibrium profile at $T = T_o$, that is $c = c_o = c(T_o)$. With these approximations the momentum equation reads

$$\nabla^2 (\nabla^2 \psi - k^2 \psi) = \frac{\sqrt{2}}{\zeta C} \nabla \times \mu \nabla c_o , \tag{4.48}$$

with μ given by equation (4.31).

First we will consider a planar interface with a temperature gradient parallel to it, as schematically depicted in figure 4.2 on the left hand side. The direction of the temperature gradient is indicated by the arrow. The temperature gradient induces an interfacial tension gradient in the opposite direction, which causes stretching of the interface at higher temperatures and shrinkage a lower temperature. This process also induces a velocity in the surrounding fluid. The right hand side of figure 4.2 shows the classical and the diffuse-interface
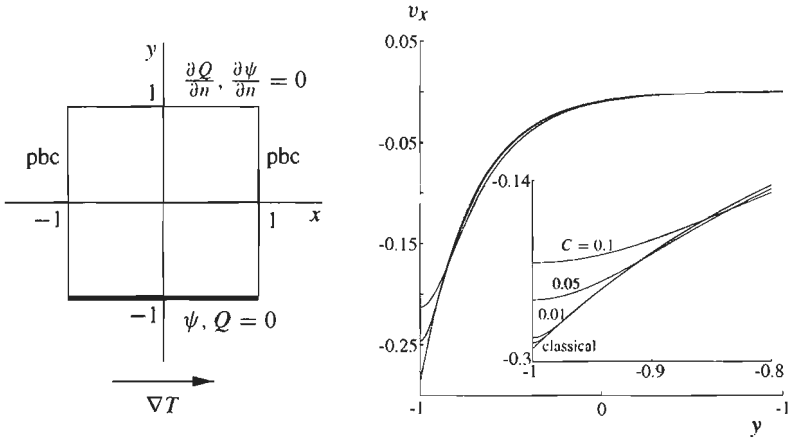
Figure 4.2: *Planar interface, located at $y = -1$, with a temperature gradient parallel to it (left)
and the resulting thermo-capillary flow (right): classical and diffuse-interface for $C =$
$0.1, 0.05, 0.01, 0.005$.*

results for this thermo-capillary flow. The classical result is $v_x(y) = -\exp(-\sqrt{12}y)/\sqrt{12}$.
The diffuse-interface result for $C = 0.1, 0.05, 0.01, 0.005$ are shown. The diffuse-interface
results were obtained by solving equation (4.48) with $c_o = \tanh((y+1)/(\sqrt{2}C))$. In the ab-
sence of a lateral length scale we have chosen $L = b$. The inset picture in figure 4.2 shows the
flow near the interface in more detail. The results show a clear convergence to the classical
solution for $C \to 0$.

The second case we consider is thermo-capillary flow in and outside a circular droplet, as
depicted in figure 4.3. The radius of the droplet is used as the length scale. The temperature
gradient again causes stretching at $x = 1$ and shrinkage at $x = -1$. This will induce a flow
in and outside the droplet with a streamline pattern as shown in figure 4.4. The classical
(top row) and the diffuse-interface results (bottom row) for the streamline pattern are shown
for $k = 2\sqrt{12}$ and $k = 20\sqrt{12}$, where we used $C = 0.01$. The pattern inside the droplet
matches the classical result. The pattern outside the droplet differs from the classical result,
because the classical results were obtained on an infinite domain whereas we used a finite
domain for the diffuse-interface calculations. Therefore, the flow field far away from the
droplet is different, but the flow field in the vicinity of the droplet matches the classical
result. The top right picture in figure 4.3 shows ψ inside the droplet for $x = 0, 0 \le y \le 1$,
where we used $k = 10\sqrt{12}$. The classical result and the diffuse-interface results for $C =$
$0.1, 0.05, 0.01, 0.005, 0.001$ are shown. Again, we find a clear convergence to the classical
solution for $C \to 0$. There is a good match if C is smaller than the thermo-capillary boundary
layer $\delta \sim k^{-1}$.

In this section we have only considered pinned interfaces. If the contact lines of the
droplet were freely movable the droplet would migrate towards higher temperatures. This
process was investigated by Jasnow and Viñals (1996). In the next section we will consider
a freely movable interface with a temperature gradient perpendicular to it and we investigate
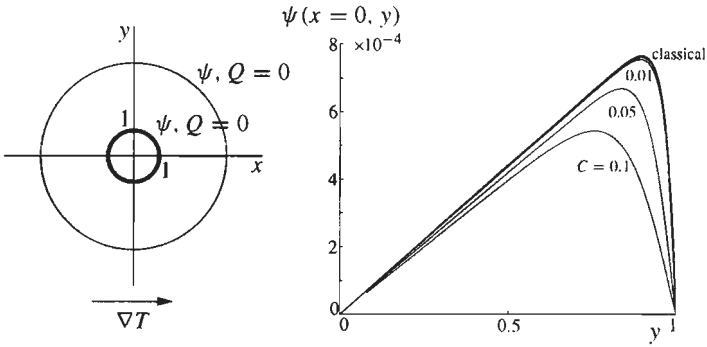how this affects the stability of the interface.

Figure 4.3: *Circular droplet with a temperature gradient in the x direction (left) and the results for the thermo-capillary flow (right): classical and diffuse-interface for C = 0.1, 0.05, 0.01, 0.005, 0.001.*

$$k = 2\sqrt{12} \qquad\qquad k = 20\sqrt{12}$$
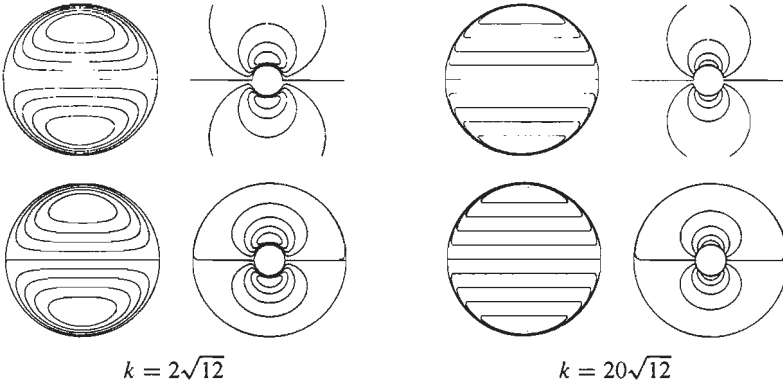
Figure 4.4: *Classical results (top) and diffuse-interface results (bottom) for the flow field in and outside the droplet for $k = 2\sqrt{12}$ and $k = 20\sqrt{12}$. In both cases $C = 0.01$ was used.*

4.6 Thermo-capillary instabilities

Consider an interface with a temperature gradient perpendicular to it as depicted in figure 4.5. A small perturbation in the interface towards the high temperature side now leads to local stretching of the interface. We shall see that this can lead to a destabilising Marangoni convection.

In the diffuse-interface approach interfacial tension is fixed by the choice of the equation of state. Therefore, we can only vary the interfacial tension by varying temperature. However, the dependence of interfacial tension on temperature can be different for another choice of fluids. We now assume that the momentum equation for other systems can still be written in the form of equation (4.48), but we replace ζ by an independent parameter $\tilde{\zeta}$. This way we can choose the ratio of the interfacial tension gradients and interfacial tension independent of the temperature gradient. Again assuming that ζ is small, we can now write the governing
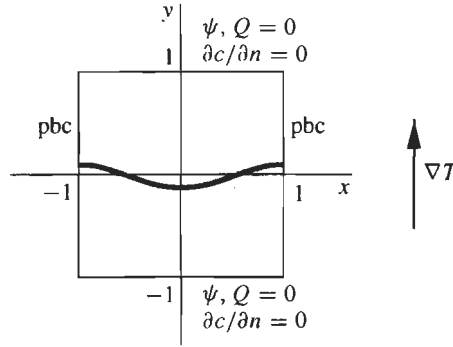
Figure 4.5: *A perturbed interface with a temperature gradient perpendicular to it.*

equations as

$$\frac{dc}{dt} = \frac{1}{Pe}\nabla^2 \mu_o \tag{4.49}$$

$$\nabla^2(\nabla^2\psi - k^2\psi) = \frac{\sqrt{2}}{\tilde{\zeta}C}\nabla \times (\mu_o + \tilde{\zeta}yc)\nabla c . \tag{4.50}$$

One the advantages of this choice of the governing equations is that we can use simple homogeneous Neumann boundary conditions, that is $\partial c/\partial n = 0$, to ensure mass conservation.

Figure 4.6 shows the time development of an interface with an initial perturbation as depicted in figure 4.5 for two values of $\tilde{\zeta}$. For $\tilde{\zeta} = 0.1$ the interfacial tension gradients are
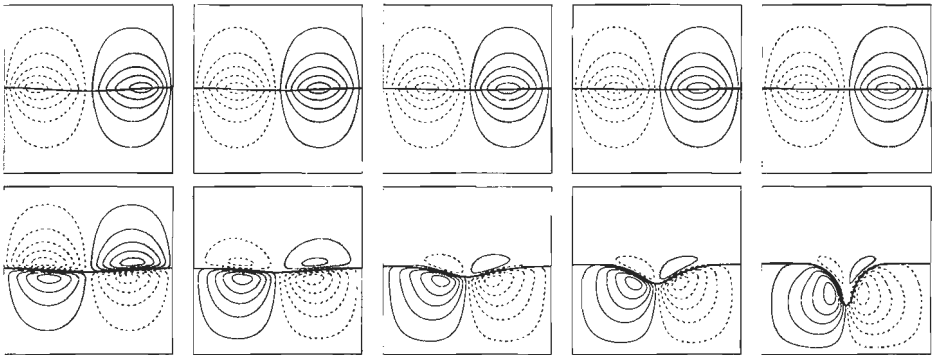
Figure 4.6: *Time development ($t = 0, 150, 250, 400, 500$) of a perturbed interface with a temperature gradient perpendicular to it for $\tilde{\zeta} = 0.1$ (top) and for $\tilde{\zeta} = 10$ (bottom). We used $k = 10\sqrt{12}$, $Pe = 10^4$ and $C = 0.01$. The streamlines are also shown: for the solid lines the motion is clockwise and for the dashed lines counterclockwise.*

too weak compared to interfacial tension itself and a stabilising motion sets in. For $\tilde{\zeta} = 10$ the interfacial tension gradients dominate and the perturbation grows. For larger values of k

the system would be unstable for smaller values of $\tilde{\zeta}$, but the thermo-capillary boundary layer is more difficult to capture for large values of k since we have to use $C < k^{-1}$ to obtain the correct results.

The observed instability is different from Rayleigh-Bénard instabilities (Davis, 1987), since we did not include heat convection due to fluid motion. Heat convection would have a stabilising effect on the instability shown in figure 4.6: the convection cells would transport low temperature to regions of low tension and high temperature to regions of high tension.

As stated above, the choice of a small value for k has forced us to use a large value of $\tilde{\zeta}$ to get the system unstable. For most binary fluid systems interfacial tension depends only weakly on temperature, as predicted by equation (4.28). However, for near-critical systems interfacial tension itself drops to zero. Using equation (4.28) we find $\gamma^{-1} d\gamma/dT \sim (T_c - T)^{-1}$. This shows that, for $T \to T_c$, the interfacial tension gradients can easily dominate.

Finally, we show the time development of a planar interface with small random perturbation (see figure 4.7). The resulting instability is similar to the one observed in figure 4.6.
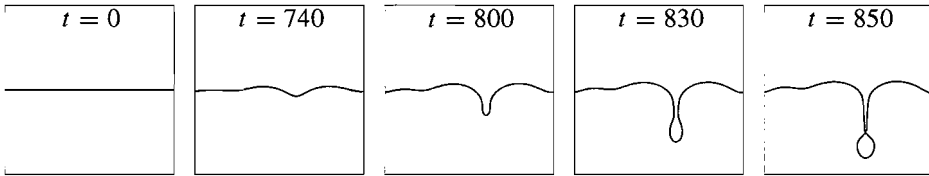

Figure 4.7: *Time sequence of a randomly perturbed interface with a temperature gradient perpendicular to it for $\tilde{\zeta} = 20$, $k = 10\sqrt{12}$, $Pe = 10^4$ and $C = 0.01$.*

The interfacial deformation is so strong that a droplet pinches off. Strong interfacial deformations as in figure 4.6 were also observed in other systems with low interfacial tension and high interfacial tension gradients. For example, adding a small amount of solvent to the binary system can induce large interfacial tension gradients if the interfacial tension depends strongly on the solvent concentration. This situation can lead to what Sternling and Scriven have called 'interfacial turbulence' (Sherwood and Wei, 1957; Sternling and Scriven, 1959). Also some polymer-solvent-nonsolvent systems, in which interfacial tension depends strongly on the solvent concentration, show this kind of interfacial deformation, often referred to as macrovoid formation (Berghmans, 1995).

Figure 4.6 also shows that we can also handle topological changes in the interface. However, the pinch-off also introduces another length scale, which is related to the thickness of the drainage layer before pinch-off. This length scale is often smaller than the size of thermocapillary boundary layer. To get correct results for the pinch-off we have to choose C smaller than this length scale. For too large values of C the pinch-off time will be underestimated (Lowengrub and Truskinovsky, 1998).

4.7 Conclusions

In this chapter we have presented the diffuse-interface approach to thermo-capillary flow. A Galerkin type spectral element discretisation, based on Gauss-Lobatto quadrature, was used

for numerical implementation of the governing equations. The high-order spectral interpol-
ation is very suitable for an accurate capturing of small interfacial thicknesses (Verschueren
et al., 1998).

The computational results were compared directly to analytical classical results. The
diffuse-interface result converges to the classical results for $C \to 0$. The results shows that,
to obtain a sufficiently accurate match with the sharp-interface result, we do not have to use
the physical value for the interfacial thickness. Sufficiently accurate results were obtained
when C is smaller than the thermo-capillary boundary layer $\delta \sim k^{-1}$.

Finally, the effect of a temperature gradient perpendicular to an interface on the stability
of the interface was investigated. The interface is unstable for systems in which interfacial
tension gradients dominate interfacial tension. The results are in qualitative agreement with
the linear stability analysis presented by Boos and Thess (1997). The results also show that
diffuse-interface model is very suitable for modelling instabilities causing large interfacial
deformations and even topological changes. However, to obtain correct results in case of
droplet pinch-off C has to be sufficiently smaller that the layer thickness just before pinch-
off. This length scale is often much smaller than the size of the thermo-capillary boundary
layer.

Chapter 5

COALESCENCE IN HYPERBOLIC FLOWS

5.1   Introduction

Coalescence of fluid domains is a frequently encountered phenomenon in industrial processing and modern technologies (e.g. Edwards *et al.*, 1991). Consequently, it is a much studied subject in literature nowadays (e.g. Chesters, 1991). In the classical approach the interface between the fluids is represented by a discontinuity in the concentration and appropriate boundary conditions are applied to connect the bulk phases (Landau and Lifshitz, 1959). This approach makes it very difficult, both physically and numerically, to handle the topological transitions which occurs during coalescence. Classical studies, therefore, mainly focus on the drainage of the film in between the fluid domains and it is assumed that coalescence takes place when the film reaches a certain critical size for which the intermolecular forces become important (e.g. Bazhlekov *et al.*, 1999).

The most 'natural' numerical technique for the classical, sharp-interface approach, is the front tracking method (Hyman, 1984; Unverdi and Tryggvason, 1992): the discretisation is such that the grid points follow the interface. In case the topology of the interface changes, complicated re-meshing (interface 'surgery') is necessary. In an attempt to overcome this problem Brackbill *et al.* (1991) proposed a continuum surface force method, in which the sharp-interface is replaced by a continuous 'colour' function. This approach generally allows to pass the topological transition. However, the 'colour' function is an arbitrary function without a clear physical meaning, which makes it difficult to physically justify the computed topological change.

In the diffuse-interface approach, which goes back to the ideas of Van der Waals (van der Waals, 1979), the interface also has a finite thickness, but it is no longer arbitrary: it is determined by the molecular force balance at the interface and its value is closely related to the finite range of molecular interactions (Rowlinson and Widom, 1989). Thermodynamic-

ally, the finite interaction range is represented by a non-local effect in the free energy of the system: the local free energy not only depends on the local concentration, but also on the concentration of the immediate environment (Davis and Scriven, 1982). By using a Taylor expansion of the free energy about the homogeneous state, the non-local effect can be represented by a dependence on local composition gradients instead of non-local composition (Cahn and Hilliard, 1958). Non-classical expressions for the chemical potential and the stress tensor can then be derived in differential form (Davis and Scriven, 1982), which makes it easy to couple them with the equations of fluid dynamics.

The molecular force balance at the interface also controls the topological transition. Therefore, the diffuse-interface methods allow to pass the topological transition in a physically justified way. The diffuse-interface approach has been used to study a wide range on phenomena involving topological changes: e.g. nucleation (Bates and Fife, 1993; Dell'Isola *et al.*, 1996), spinodal decomposition (Gurtin *et al.*, 1996), droplet breakup (Jacqmin, 1996). For a review on the subject see Anderson *et al.* (1998). Most of the papers on topological changes focus on small-scale systems, in which it is assumed that the numerical interfacial thickness is very close to the real interfacial thickness or little attention is being paid to the dependence on the choice of the interfacial thickness. For large scale systems, for which the droplet size is much larger than the physical value of the interfacial thickness, the real interfacial thickness can not be captured numerically, in general. The scaling in such systems needs special attention, because if the real interfacial thickness is to be replaced by a numerically acceptable thickness, we have to make sure that we are still describing the same system with the same interfacial tension and diffusion. In their paper on coalescence in thin, unstably stratified fluid layers in a Hele-Shaw cell, Lowengrub *et al.* (1998) investigated the dependence on the value of the interfacial thickness. They used a scaling for which the diffuse-interface equations reduce to the classical sharp-interface model in the limit of zero interfacial thickness (Lowengrub and Truskinovsky, 1998). For small values of the dimensionless interfacial thickness, they found that the drainage layer breaks up into droplets. They also found a good agreement with classical results. Here, we propose an alternative scaling which is not based on obtaining the classical equations in the sharp-interface limit: it is assumed that the diffuse-interface equations yield the correct results when the real interfacial thickness is used. The real interfacial thickness is then replaced by a numerically larger one, where the scaling is such that interfacial tension is kept constant. Lowengrub and Truskinovsky (1998) used a similar argument to scale their capillary terms. For the Peclet number they used a scaling which allowed them to obtain the classical, sharp-interface model in the limit of zero interfacial tension. We use the same arguments, which are used to scale the capillary term, to scale the diffusion term. This yields a different scaling for the Peclet number.

We study coalescence in hyperbolic flows, for droplets in a Hele-Shaw cell and for cylinders in two-dimensional flows. In section 5.2 we define the system to be investigated. Section 5.3 is devoted to the diffuse-interface theory and the scaling. In section 5.4 we briefly discuss the computational methods. In section 5.5 the results are presented. First, we discuss coalescence in a Hele-Shaw geometry for density- and viscosity-matched fluids using the same scaling as used by Lowengrub and Truskinovsky (1998). Next, we investigate the effect of the alternative scaling for the Peclet number mentioned above. After that, we briefly discuss systems for which the droplet viscosity differs from the viscosity of the surrounding liquid.

To conclude, we consider coalescing cylinders. Finally, section 5.6 contains some discussion and concluding remarks.

5.2   System definition

Consider the coalescence of two fluid domains in a hyperbolic flow as schematically depicted in figure 5.1. We will consider two cases: coalescing droplets in a Hele-Shaw geometry and
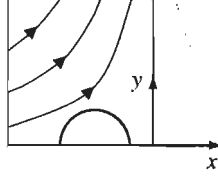

Figure 5.1: Schematic picture of two droplets (cylinders) in a hyperbolic flow.

coalescing cylinders. The density of the droplets (cylinders) and the surrounding liquid is the same. The viscosity of the droplets (cylinders) is η_d and the viscosity of the surrounding liquid is η_c. The droplets (cylinders) are subject to a hyperbolic flow of the form $v = A(-x, y)$, where A is a constant. Assuming the flow is symmetric[1], we only use the top-left part of the domain (see figure 5.1) for the computations.

Neglecting inertia, the equations governing the coalescence of two density-matched cylinders are given by the two-dimensional Stokes equations, which read

$$\nabla \cdot v = 0 , \tag{5.1}$$
$$\nabla \cdot \tau = 0 , \tag{5.2}$$

where $\nabla = (\partial/\partial x, \partial/\partial y)$, v is the velocity and $\tau = -p\mathsf{I} + \eta(\nabla v + \nabla v^\mathsf{T})$ is the Cauchy stress tensor with pressure p and shear viscosity η. In the classical approach, the appropriate boundary conditions are applied at the interface between the two fluids to connect the bulk phases. The kinematic and the stress boundary condition are (Landau and Lifshitz, 1959)

$$[\![v]\!] = 0 , \tag{5.3}$$
$$[\![\tau \cdot \hat{n}]\!] = \gamma \hat{n} \nabla_s \cdot \hat{n} , \tag{5.4}$$

where $\hat{n}$ is the unit vector normal to the interface, $\nabla_s = (\mathsf{I} - \hat{n}\hat{n}) \cdot \nabla$ denotes the interface gradient and γ is the interfacial tension, which is assumed to be constant. The kinematic boundary condition ensures that the velocity is continuous across the interface and the stress boundary condition relates interfacial tension to a jump in the normal stress. However, as

---

[1] In reality the head-on collision of droplets is not stable, tumbling can occur.

stated in the previous section, the necessity to apply these boundary conditions is very inconvenient in case of topological changes. In the diffuse-interface approach, which will be presented in the next section, interfacial tension is included as a body force in the momentum equation. Consequently, a direct application of boundary conditions is no longer required.

A Hele-Shaw geometry consist of two, closely spaced parallel plates. We assume that the contact lines of the interface between the fluids, which touch both plates, can move freely. Neglecting the small-scale flow near moving contact lines (Dussan V and Davis, 1974; Jacqmin, 1996; Seppecher, 1996), the flow in between the plates can be assumed to be a Poisseuille flow. Using the parabolic Poisseuille velocity profile, the three-dimensional momentum equation can be averaged over the gap between the plates. This yields the Darcy equation (Saffman and Taylor, 1958):

$$\nabla p = -\frac{12\eta}{b^2} v \, , \tag{5.5}$$

where b is the plate spacing and v is now the velocity averaged over the gap. The term on the right hand side takes into account the friction force of the flow due to the presence of the plates.

5.3   Diffuse-interface theory

The governing equations can be derived from a variational principle in which the Lagrangian takes the following form (Lowengrub and Truskinovsky, 1998)

$$\mathcal{L} = \int_{t_1}^{t_2} \int_{\Omega} \rho(\tfrac{1}{2}|v|^2 - f) \, d^3 r dt \, , \tag{5.6}$$

where f is the specific Helmholtz free energy. As mentioned in the first section, the essential ingredient of diffuse-interface modelling is the non-local effect in the free energy, which can be represented by a dependence on local concentration gradients. Using $f = f(\rho, c, \nabla c)$, where c is the mass fraction of one of the components, Lowengrub and Truskinovsky (1998) obtained generalised relations for the chemical potential and the reversible part of the stress tensor for quasi-incompressible systems. For density-matched fluids their results read[2]

$$\mu = \frac{\partial f}{\partial c} - \nabla \cdot \frac{\partial f}{\partial \nabla c} \, , \tag{5.7}$$

$$\tau_r = -p\mathsf{I} - \rho \frac{\partial f}{\partial \nabla c} \nabla c \, , \tag{5.8}$$

where μ is the generalised chemical potential and τ_r is the reversible part of the stress tensor. Cahn and Hilliard (1958) derived the following form for the specific Helmholtz free energy

$$f(c, \nabla c) = f_0(c) + \tfrac{1}{2}\epsilon|\nabla c|^2 \, , \tag{5.9}$$

---

[2] Note that exactly the same results were obtained in section 2.7 of this thesis.

where c is the mass fraction of one of the components, f_0 is the homogeneous part of the specific Helmholtz free energy and ϵ is the gradient energy parameter, which is assumed to be constant. The homogeneous part f_0 can be specified by using a Taylor expansion about the critical point $c = c_c$. This way we obtain the so-called 'c^4' approximation (Gunton *et al.*, 1983): $f_0(\tilde{c}) = \frac{1}{4}\beta\tilde{c}^4 - \frac{1}{2}\alpha\tilde{c}^2$, where $\tilde{c} = c - c_c$. For isothermal systems below the critical temperature, the parameters α and β are both positive constants. In this case, f_0 has the shape of a double well potential. Omitting the tilde notation, f can now be written as[3]

$$f(c, \nabla c) = -\tfrac{1}{2}\alpha c^2 + \tfrac{1}{4}\beta c^4 + \tfrac{1}{2}\epsilon |\nabla c|^2 \,, \tag{5.10}$$

Consequently, the chemical potential reads

$$\mu = -\alpha c + \beta c^3 - \epsilon \nabla^2 c \,. \tag{5.11}$$

This generalised chemical potential allows us to describe the interface between the two fluids by a continuously varying concentration profile. For example, for a planar interface, with x the direction normal to the interface, an analytical equilibrium solution ($\mu = 0$) can be found, which reads

$$c(x) = \sqrt{\frac{\alpha}{\beta}}\tanh\frac{x}{\sqrt{2}\xi} \quad \text{with } \xi = \sqrt{\frac{\epsilon}{\alpha}} \,, \tag{5.12}$$

where $\pm\sqrt{\alpha/\beta}$ are the equilibrium bulk solutions and ξ is a measure for the interfacial thickness.

Assuming that the diffusion flux is proportional to the gradient of the generalised chemical potential the local balance equation for the mass fraction c can be written as

$$\rho\frac{dc}{dt} = M\nabla^2\mu \,, \tag{5.13}$$

where M is the mobility coefficient, which is assumed to be constant. This relation is known as the Cahn-Hilliard equation (Cahn and Hilliard, 1959) and was originally used to describe the initial stages of spinodal decomposition (Cahn, 1964). In our case, it allows us to transport the continuous interface profiles between the two fluids in a velocity field.

Adding the viscous stress tensor to the reversible part of the stress tensor (5.8) we obtain the non-classical extra stress tensor. The non-classical Stokes equations can then be written as

$$\nabla \cdot v = 0 \,, \tag{5.14}$$

$$\nabla p = -\rho\epsilon\nabla\cdot(\nabla c\nabla c) + \nabla\cdot[\eta(\nabla v + \nabla v^{\mathsf{T}})] \,. \tag{5.15}$$

The first term on the right hand side of equation (5.15) can be rewritten as $\rho\epsilon\nabla\cdot(\nabla c\nabla c) = \rho\nabla f - \rho\mu\nabla c$ (Lowengrub and Truskinovsky, 1998). Consequently, we obtain

$$\nabla g = \rho\mu\nabla c + \nabla\cdot[\eta(\nabla v + \nabla v^{\mathsf{T}})] \,, \tag{5.16}$$

---

[3] The 'c^4' approximation is discussed in more detail in chapter 3, section 3.2.

where $g = f + p/\rho$ is the specific Gibbs free energy.

For viscosity-matched fluids it is convenient to rewrite the Stokes equations in terms of the stream function ψ, which is defined by $\boldsymbol{v} = (\partial\psi/\partial y, -\partial\psi/\partial x)$. This way mass conservation is automatically satisfied and the local balance equation for ψ is obtained by taking the curl of equation (5.16). This yields

$$\eta\nabla^4\psi = \rho\nabla\times\mu\nabla c , \tag{5.17}$$

where $\nabla\times$ denotes the curl. For a Hele-Shaw geometry the viscous term is replaced by the Darcy term, as in equation (5.5). In this case, we can also use the stream function formulation in case the viscosities are not equal. We obtain the following generalised Darcy equation

$$-k^2\nabla\cdot(\eta\nabla\psi) = \rho\nabla\times\mu\nabla c , \tag{5.18}$$

where $k^2 = 12/b^2$ is the permeability of the cell.

To write the governing equations in a non-dimensional form we use the following dimensionless variables: $c^* = c/c_B$, $r^* = r/L$, $\boldsymbol{v}^* = \boldsymbol{v}/V$, $\mu^* = \mu\xi^2/(\epsilon c_B)$, $t^* = tV/L$, $\eta^* = \eta/\eta_d$ and $\psi^* = \psi/(LV)$, where $c_B = \sqrt{\alpha/\beta}$ is the equilibrium bulk concentration, L is the radius of the droplet (cylinder) and we choose $V = 10AL$. Omitting the asterisk notation we obtain the following dimensionless governing equations for the coalescing cylinders, which have the same viscosity as the surrounding liquid

$$\frac{dc}{dt} = \frac{1}{Pe}\nabla^2\mu \quad \text{with} \quad \mu = c^3 - c - C^2\nabla^2 c , \tag{5.19}$$

$$\nabla^4\psi = \frac{1}{Ca}\frac{1}{C}\nabla\times\mu\nabla c . \tag{5.20}$$

For droplets in a Hele-Shaw geometry, the non-dimensional generalised Darcy equation reads

$$-k^2\nabla\cdot(\eta\nabla\psi) = \frac{1}{Ca}\frac{1}{C}\nabla\times\mu\nabla c , \tag{5.21}$$

where $k^2 = 12L^2/b^2$ is now the dimensionless permeability. The dimensionless groups appearing in the governing equations: the Peclet number Pe, the capillary number Ca and the Cahn number C are defined by

$$Pe = \frac{\xi^2 LV}{M\epsilon} \quad Ca = \frac{\xi\eta_d V}{\rho\epsilon c_B^2} \quad \text{and} \quad C = \frac{\xi}{L} , \tag{5.22}$$

respectively.

The capillary number can be related to the classical definition, $Ca_{\text{cl}} = \eta_d V/\gamma$, by considering the interfacial tension γ for a planar interface. Interfacial tension can be defined as the excess tangential stress (Davis and Scriven, 1982):

$$\gamma = \int_{-\infty}^{\infty} \hat{\boldsymbol{n}}\cdot(\boldsymbol{\tau}_r\cdot\hat{\boldsymbol{n}} - \boldsymbol{\tau}_r\cdot\hat{\boldsymbol{i}})dx = \rho\epsilon\int_{-\infty}^{\infty}(dc/dx)^2 dx , \tag{5.23}$$

where $\hat{\boldsymbol{n}}$ and $\hat{\boldsymbol{t}}$ are the unit vectors normal and tangential to the interface, respectively. Using the equilibrium profile (5.12) we obtain

$$\gamma = \frac{2\sqrt{2}}{3} \frac{\rho \epsilon c_B^2}{\xi} .$$ (5.24)

Consequently, the capillary number can be rewritten as

$$Ca = \frac{2\sqrt{2}}{3} \frac{\eta_d V}{\gamma} ,$$ (5.25)

which shows that $Ca/Ca_{\mathrm{cl}} = 2\sqrt{2}/3$.

Considering the sharp-interface limit, Lowengrub and Truskinovsky (1998) argued that the scaling should be such that a finite value for the interfacial tension is obtained when taking $C \to 0$. Equation (5.24) shows that this is the case if we keep $\epsilon c_B^2/\xi$ constant. In their paper Lowengrub and Truskinovsky (1998) used $c_B = 1$ and their scaling is, therefore, equivalent to keeping ϵ/ξ constant. For the Peclet number they used $Pe = 1/C$. Using matched asymptotics, they showed that the diffuse-interface equations reduce to the classical sharp-interface. However, keeping ϵ/ξ constant in the Peclet number defined in (5.22), yields a Peclet number which is proportional to C rather than $1/C$, if the other parameters are kept constant. We will investigate the difference between these scalings for the Peclet number.

In summary: the governing equations for the coalescing cylinders are given by equations (5.19) and (5.20). For the Hele-Shaw system, equation (5.20) is replaced by the generalised Darcy equation (5.21), which has to be supplemented with an equation which specifies η as a function of c, in case the fluids are not viscosity-matched.

Analytical solutions, for these sets of equations, can only be obtained in some special cases. In general, a numerical implementation is needed. This is the subject of the next section.

5.4 Computational methods

To discretise the governing equations we use a spectral element method (Patera, 1984; Timmermans *et al.*, 1994). Due to the high order of approximation, this method is expected to be especially suitable for capturing interfaces with a small interfacial thickness (Verschueren *et al.*, 1998). The computational domain Ω is divided into N_{el} non-overlapping sub-domains Ω_e and a spectral approximation is applied on each element. Figure 5.2 shows the computational domain with a typical element distribution. The basis functions ϕ, which are used for the spatial discretisation, are high-order Lagrange interpolation polynomials through the Legendre-Gauss-Lobatto integration points defined per element.

The Galerkin weighted residual representation of the generalised Darcy equation (5.21) is

$$-k^2(\nabla^2\psi, w)_\Omega = (h, w) ,$$ (5.26)

where $h = Ca^{-1}C^{-1}\nabla \times \mu \nabla c$, the inner product $(a, w)_\Omega = \int_\Omega awd^2\boldsymbol{r}$ and w is the standard Galerkin test function. Partial integration yields the weak or variational form

$$k^2(\nabla^2\psi, w)_\Omega = (h, w) ,$$ (5.27)

$$\psi = x/2.5, c = -1, \mu = 0$$

$$\psi = y/2.5$$
$$c = -1, \mu = 0$$

$$\psi = 0$$
$$\frac{\partial c}{\partial n} = 0, \frac{\partial \mu}{\partial n} = 0$$

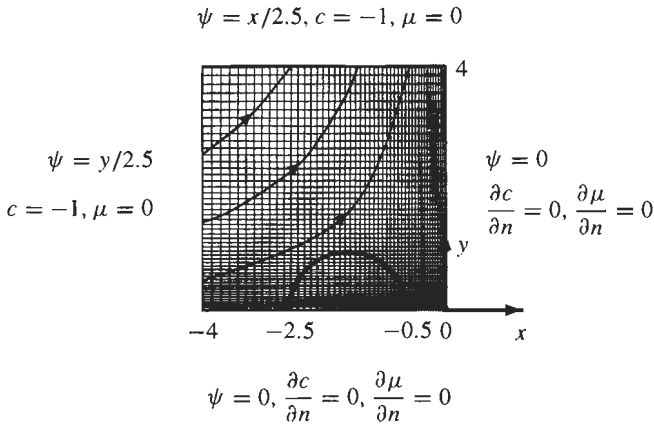$$\psi = 0, \frac{\partial c}{\partial n} = 0, \frac{\partial \mu}{\partial n} = 0$$

Figure 5.2: Schematic picture of the computational domain with a typical mesh and the appropriate boundary conditions.

where the boundary integrals vanish because of the homogeneous boundary conditions (see figure 5.2). Next, the total domain Ω is decomposed into N_{el} non-overlapping sub-domains Ω_e and a spectral approximation is applied on each element. After assembling the elements we obtain the following discrete form for the Darcy equation

$$-\mathbf{S}_\eta \boldsymbol{\psi} = \mathbf{M}\boldsymbol{h} , \tag{5.28}$$

where $\mathbf{S}_\eta$ is the matrix representation of $k^2 \nabla \cdot \eta \nabla$, $\mathbf{M}$ is the mass matrix and $\boldsymbol{\psi}$ and $\boldsymbol{h}$ are the discrete vector representations of ψ and h, respectively.

The momentum equation governing the coalescence of cylinders, equation (5.20), is a fourth order differential equation in ψ. Since the basis functions ϕ are elements of H^1, that is $H^1(\Omega) = \{\phi \mid \phi \in L^2(\Omega), \nabla\phi \in L^2(\Omega) \times L^2(\Omega)\}$, we split up equation (5.20) into two second order differential equations

$$\nabla^2 Q = h , \tag{5.29}$$
$$\nabla^2 \psi = Q . \tag{5.30}$$

Using the same procedure as for the Darcy equation, after spatial discretisation we obtain

$$\mathbf{S}Q = \mathbf{M}\boldsymbol{h} , \tag{5.31}$$
$$\mathbf{S}\boldsymbol{\psi} = \mathbf{M}Q . \tag{5.32}$$

The local balance equation for c and the chemical potential also form a set of two second order differential equations, which we will solve in a coupled way. Besides spatial discretisation we now also need temporal discretisation. Using the Euler implicit method for time

discretisation and the same spatial discretisation as for the momentum equation we obtain

$$
\begin{bmatrix}
\mathbf{M} - \Delta t \mathbf{N}^n & \dfrac{\Delta t}{Pe}\mathbf{S} \\[2ex]
[1 - (c_i^{n+1})^2]\mathbf{M} - C^2\mathbf{S} & \mathbf{M}
\end{bmatrix}
\begin{bmatrix}
c_{i+1}^{n+1} \\[2ex]
\mu_{i+1}^{n+1}
\end{bmatrix}
=
\begin{bmatrix}
\mathbf{M}c_0^n \\[2ex]
0
\end{bmatrix},
\tag{5.33}
$$

where $\mathbf{N}$ is the convection matrix, where $v = (\partial\psi/\partial y, -\partial\psi/\partial x)$ is used to compute the velocity field. Superscript n denotes time t and $n+1$ denotes $t + \Delta t$. A Picard iteration is used to deal with the nonlinear term (subscript $i = 1 \ldots I$): the iteration starts using $c_1^{n+1} = c_0^n$ and as a stopping criterion we use $\max|c_{I+1}^{n+1} - c_I^{n+1}| < 10^{-4}$. After convergence, μ_{I+1}^{n+1} and c_{I+1}^{n+1} are used to compute a new h and we can move to the next time step.

5.5   Results

In this section we present the diffuse-interface results for coalescence in hyperbolic flows. First, we investigate the difference between the two different scalings for the Peclet number, as discussed in section 5.3, for coalescence in a Hele-Shaw cell. Secondly, we show the results for different viscosity ratios and, finally, we compare the results for coalescing cylinders to classical results.

Figure 5.3 shows a time sequence of two coalescing droplets, in a Hele-Shaw cell for $C = 0.06$ (top) and $C = 0.1$ (bottom), where we used $Pe = 1/C$, $Ca = 0.01$ and $\Delta t = 0.01$ in both cases. The density and viscosity of the surrounding liquid is equal to the density and the viscosity of the droplets. The thick solid line is the $c = 0$ contour line and the thin lines represent the vorticity, where the solid lines correspond to clockwise flow and the dashed lines to counterclockwise flow. The vorticity of a hyperbolic flow, $v \sim (-x, y)$, equals zero.
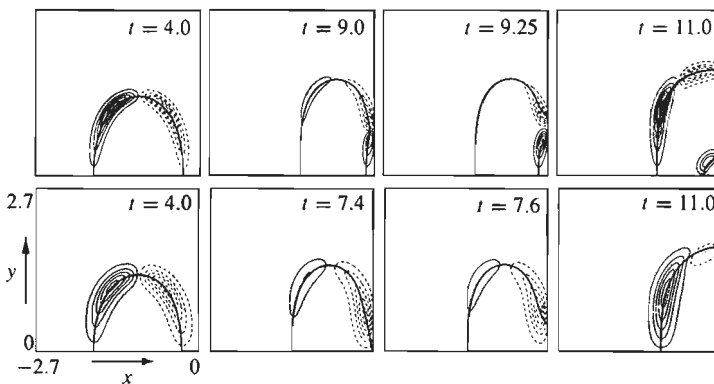

Figure 5.3: Time sequence for $C = 0.06$ (top) and $C = 0.1$ (bottom), where $Ca = 0.01$ and $Pe = 1/C$.

Furthermore, equation (5.21) shows that there is no production of vorticity in the absence of viscosity gradients, interfacial tension and diffusion. Therefore, for viscosity-matched
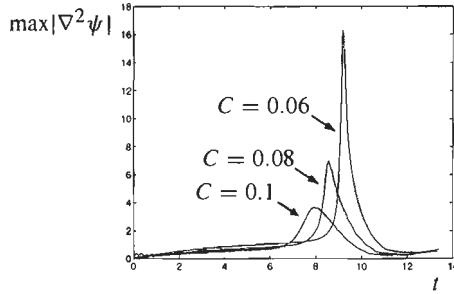
$\max|\nabla^2\psi|$

Figure 5.4: *Maximum vorticity as a function of time for* $C = 0.1, 0.08, 0.06$ *where* $Ca = 0.01$ *and* $Pe = 1/C$.

systems, the vorticity is a measure for the effect of diffusion and interfacial tension on the system. The pictures on the left hand side, at $t = 4$, clearly show that the droplets are resisting to the deformation induced by the hyperbolic flow. At this time the results look similar, but when coalescence occurs we see large differences in both the vorticity and the concentration: the top sequence shows dimple forming, which is typical for coalescence of droplets (e.g. Bazhlekov *et al.*, 1999), with the corresponding vorticity production, whereas in the bottom sequence coalescence occurs at $y = 0$ and there is no counterflow. Figure 5.4 shows the maximum vorticity as a function of time for $C = 0.1, 0.08, 0.06$. The peaks correspond to the vorticity production during coalescence. Even though the actual coalescence occurs just before the peak, the maximum vorticity is clearly a good measure for the coalescence time. Figure 5.4 shows that there is a relatively large spread in the coalescence time.

Now, we change the scaling of the Peclet number: instead of $Pe = 1/C$ we now use $Pe = C/0.06^2$, such that the value is the same for $C = 0.06$. Figure 5.5 shows the results for $C = 0.1$ (bottom) and $C = 0.06$ (top). The top sequence is identical to the one shown
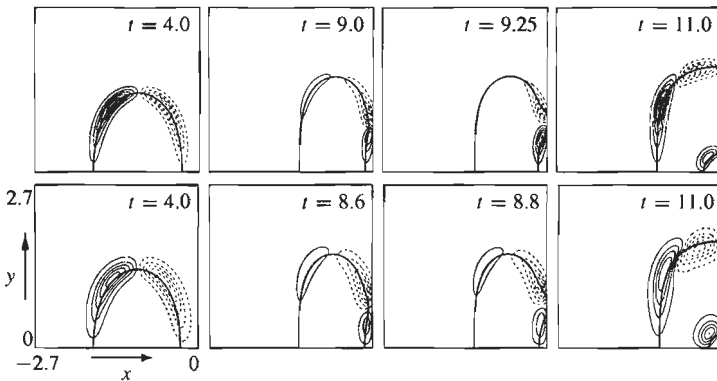

Figure 5.5: *Time sequence for* $C = 0.06$ *(top) and* $C = 0.1$ *(bottom), where* $Ca = 0.01$ *and* $Pe = C/0.06^2$.
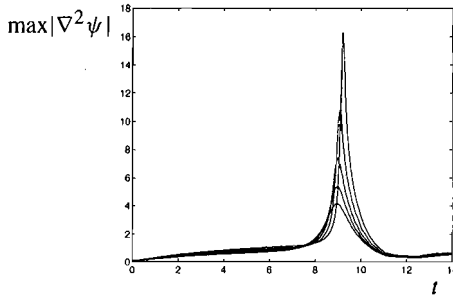
Figure 5.6: Maximum vorticity as a function of time for $C = 0.1, 0.09, 0.08, 0.07, 0.06$, where $Ca = 0.01$ and $Pe = C/0.06^2$.

in figure 5.3. The results for $C = 0.1$ are quite different from those in figure 5.3: for the new scaling the results show dimple forming with the corresponding counterflow and the observed coalescence time is also closer to the coalescence time for $C = 0.06$. The maximum vorticity as a function of time, plotted in figure 5.6, also shows this effect: the spread in the vorticity peaks is much smaller than in figure 5.4. Comparing the two scalings for the Peclet number we can conclude the following: if the interfacial thickness is replaced by a larger one, the new scaling yields a result which is much more similar to the results for the original interfacial thickness. This effect can be explained as follows. The new scaling states that, if we choose a larger interfacial thickness, the Peclet number has to be replaced by a larger one, such that the effect of diffusion is smaller. In other words, the thin interface is replaced by a thicker one for which the effect of diffusion is smaller. This way behaviour of the thicker interface is more similar the thinner one. For the $Pe = 1/C$–scaling the effect is opposite: the effect of diffusion for the thicker interface is larger.

In general, changing the droplet viscosity will affect the deformation rate and the drainage time. Figure 5.7 shows a time sequence of coalescence for two viscosity ratios: $\eta_c/\eta_d = 2$
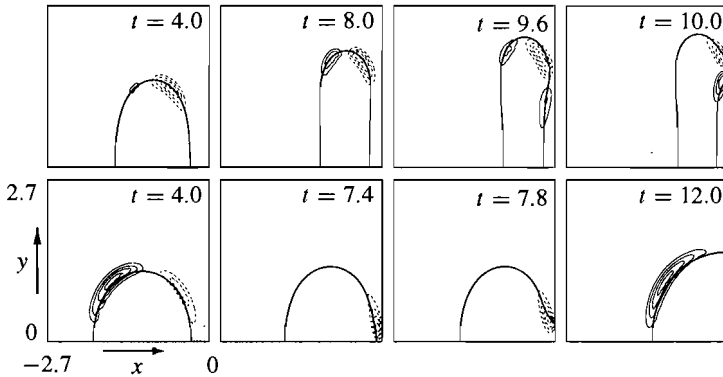

Figure 5.7: Time sequence for $\eta_c/\eta_d = 2$ (top) and $\eta_c/\eta_d = 0.5$ (bottom), where $Ca = 0.01$, $C = 0.08$ and $Pe = C/0.06^2$.
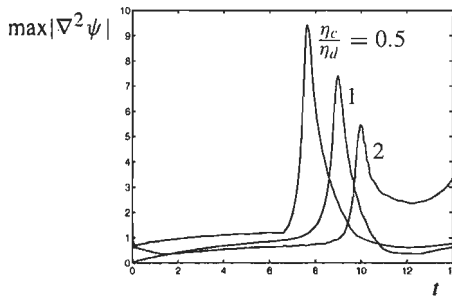
Figure 5.8: *Maximum vorticity as a function of time for* $\eta_c/\eta_d = 0.5, 1, 2$, *where* $Ca = 0.01$, $C = 0.08$ *and* $Pe = C/0.06^2$.

(top) and $\eta_c/\eta_d = 0.5$ (bottom). For the computations we used linear viscosity profiles, that is $\eta(c) = \frac{1}{2}(1 - \eta_c/\eta_d)c + \frac{1}{2}(1 + \eta_c/\eta_d)$. The other parameters are $Ca = 0.01$ and $C = 0.08$ and $Pe = C/0.06^2$. The results show a clear effect of the viscosity ratio on the coalescence process: for $\eta_c/\eta_d = 2$ deformation is larger and the layer drainage is slower. Due to these effects, coalescence occurs earlier for $\eta_c/\eta_d = 0.5$. The maximum vorticity as a function of time, plotted in figure 5.8 for various values of η_c/η_d, also shows this effect on the coalescence time. These results are in qualitative agreement with classical results on coalescence (Bazhlekov *et al.*, 1999).

Finally, we consider coalescing cylinders, again considering the two scalings for the Peclet number. Figure 5.9 shows time sequences for three different cases: $C = 0.06$, $Pe = 10^3$
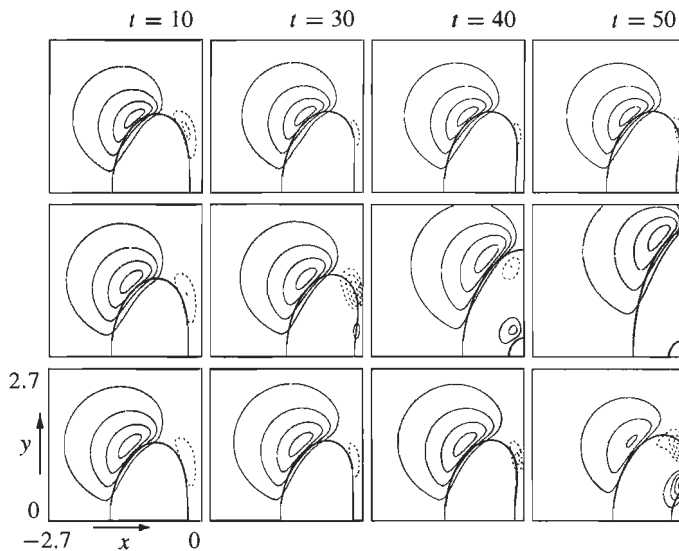

Figure 5.9: *Time sequence for* $C = 0.06$, $Pe = 10^3$ *(top),* $C = 0.1$, $Pe = \frac{0.06}{0.1}10^3$ *(middle) and* $C = 0.1$, $Pe = \frac{0.1}{0.06}10^3$ *(bottom).*
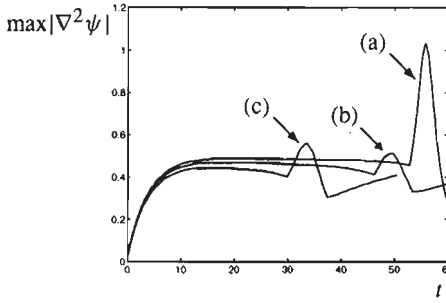
Figure 5.10: Maximum vorticity as a function of time for the three cases in figure 5.9: $C = 0.06$, $Pe = 10^3$ (a); $C = 0.1$, $Pe = \frac{0.1}{0.06}10^3$ (b); $C = 0.1$, $Pe = \frac{0.06}{0.1}10^3$ (c).

(top), $C = 0.1$, $Pe = 10^3 \cdot 0.06/C$ (middle) and $C = 0.1$, $Pe = 10^3 \cdot C/0.06$ (bottom). Furthermore, we used $Ca = 1$ and $\Delta t = 0.5$ in both cases. The scaling is the same as the one used for the Hele-Shaw system, except for $C = 0.06$ we now use $Pe = 10^3$ instead of $Pe = 1/0.06$. The cylinders shape and the vorticity pattern are different from those observed for the droplets in the Hele-Shaw geometry: the vorticity contour lines, which were localised at the interface for the Hele-Shaw geometry, now reach further into the surrounding liquid and the cylinders have a 'kidney-bean' shape which is not observed in the Hele-Shaw case. Concerning the scaling, however, we do see similarities with the Hele-Shaw results. Figure 5.10 shows the maximum vorticity as a function of time for the three time sequences displayed in figure 5.9. As for the Hele-Shaw system, we see that the result for $C = 0.1$ using the new scaling are much closer to the $C = 0.06$ result than for the other scaling. The overall spread in the vorticity peaks is larger than for the Hele-Shaw results, because we used a larger value for the Peclet number.

5.6   Discussion

We presented computational results for coalescence in hyperbolic flows using a diffuse-interface method. The diffuse-interface method allows us pass the topological transition in a physically justified way. The results for different viscosity ratios suggest that, even for the relatively large interfacial thickness used ($C = 0.08$), qualitatively correct results can be obtained.

It was argued that, if the interfacial thickness is replaced by another one, the scaling should be such that similar results are obtained. The scaling introduced in section 5.3, is such that, if an interface is replaced by another one with a larger thickness, interfacial tension is the same. Applying the same scaling to the Peclet number, we found that the Peclet number should be proportional to the Cahn number. Lowengrub and Truskinovsky (1998) used the same scaling for the capillary term to obtain a finite value for the interfacial tension in the sharp-interface limit. However, for the Peclet number they used $Pe = 1/C$. For this scaling they showed, by means of matched asymptotics, that the classical equations can be obtained in the sharp-interface limit. For a $Pe = C$–scaling it is not possible to obtain a classical Navier-

Stokes sharp-interface limit (Lowengrub and Truskinovsky, 1998). Pego (1989) showed that the classical Hele-Shaw limit can be obtained for $Pe = C$ in the sharp-interface limit, but he did not include convection in the local balance equation for the concentration. However, the proposed $Pe \sim C$-scaling is not based on obtaining the classical equations in the sharp-interface limit: it is assumed that the diffuse-interface equations yield the correct results when the real interfacial thickness is used. The real interfacial thickness is then replaced by a numerically larger one, where the scaling is such that interfacial tension is kept constant. To test if the new scaling works the results have to be compared to classical results and a larger range of interfacial thicknesses has to be considered.

The results presented in section 5.5 show that for the $Pe \sim C$-scaling the difference in the results for various values of the Cahn number C is smaller. However, there is still a difference. Further investigation is needed to check if it is possible to find a scaling for the Peclet number for which there is a perfect match.

Chapter 6

CONCLUSIONS AND RECOMMENDATIONS

In the preceding chapters the theoretical aspects of diffuse-interface theories were discussed in detail and the results of applications to several phenomena were presented: phase separation, interfacial instabilities, thermo-capillary flow and coalescence. The essential ingredient of diffuse-interface modelling is the inclusion of the range of molecular interactions, which is closely related to the interfacial thickness. Thermodynamically, this interaction range is represented by a non-local effect in the free energy of the system. The main advantage of diffuse-interface modelling over the classical, sharp-interface model is that it deals with topological interface changes, which occur during processes such as coalescence and phase separation, in a physically justified way: the range of molecular interactions, which is included in the diffuse-interface approach, controls topological changes. In general, the interfacial thickness is a small parameter, typically about 0.1 nm. A diffuse-interface model is, therefore, essentially a small-scale model. In the first part of chapter 3 and references therein, it was shown that it can be successfully applied to small-scale phenomena, such as the initial stages of phase separation, where the interfacial thickness can be captured numerically.

For large-scale systems, the interfacial thickness can not be captured numerically, in general. In this thesis we, therefore, focussed on the question whether it is possible to replace the real interfacial thickness by a numerically acceptable one and still get physically correct and accurate results. In chapter 3, section 3.3, we considered interfacial instabilities in a Hele-Shaw geometry. The results show convergence for large values of the Peclet number and small values of the dimensionless interfacial thickness, the Cahn number, which suggests that there is a sharp-interface limit (see figure 3.6). However, in this example we did not consider the scaling involved with changing the interfacial thickness.

In chapters 4 and 5 special attention has been paid to the scaling problem. It was argued that, if an interface is replaced by another one with a different thickness, the scaling of the capillary term should be such that the interfacial tension stays the same. This scaling for the capillary term was investigated in detail in chapter 4, where the diffuse-interface results for thermo-capillary flow were compared directly to classical results. Using the scaling for the capillary term which ensures that interfacial tension remains the same if we change the interfacial thickness, we found that the results for pinned linear and circular interfaces converge to the classical results for small values of the Cahn number. Sufficiently accurate results were obtained if the interfacial thickness was chosen small compared to the size of the thermo-

capillary boundary layer. In chapter 4 we also considered thermo-capillary instabilities, but for these results we kept the Cahn number and the Peclet number fixed: we used $C = 0.01$ and $Pe = 10^4$. The results for interfacial instabilities presented in chapter 3 suggest that, if we choose a smaller interfacial thickness and a larger Peclet number, the same results will be obtained. However, this is not true in case there is a topological change in the interface. In this case, the scaling of the Peclet number needs special attention. This was the topic of chapter 5.

In chapter 5 the diffuse-interface approach to coalescence in hyperbolic flows was invest-igated. The same scaling which ensures that interfacial tension stays the same if we change the interfacial thickness, was applied to diffusion. This way, we found that the Peclet number should be proportional to the Cahn number. This scaling for the Peclet number differs from the scaling used by Lowengrub and Truskinovsky (1998): they used a Peclet number which is proportional to the reciprocal of the Cahn number and they showed, by means of matched asymptotics, that the classical governing equations can be obtained in the sharp-interface limit for this scaling. In chapter 5 we compared these two scalings for the Peclet number (see fig-ures 5.3 to 5.6): the difference in the results for various values of the Cahn number using the $Pe \sim C$-scaling was much smaller than for the scaling used by Lowengrub and Truskinovsky (1998). However, the results for coalescing cylinders (see figures 5.9 and 5.10) show that for larger values of the Peclet number, there is still a relatively large difference in coalescence time if we change the Cahn number. Further research is needed to investigate what the origin of this difference is. In chapter 5 it was assumed that the phenomenological coefficients, the mobility parameter and the viscosity, are not affected by the scaling. Changing the interfacial thickness also implies a change in the interaction length, which might also affect the scaling of the phenomenological coefficients. This issue needs further investigation.

A direct comparison of diffuse-interface results to classical results for coalescence is dif-ficult, because classical results normally do not go beyond the topological change. However, there are well-established classical results on film drainage, which include intermolecular van der Waals attraction force by means of a Hamaker constant (e.g. Bazhlekov *et al.*, 1999; Rother *et al.*, 1997), which can be used as a reference. Computationally, the comparison is also more difficult than for the thermo-capillary flow in chapter 4, since we are now deal-ing with moving interfaces and we have to include the local concentration balance equation, which can lead to computational difficulties.

Firstly, the scaling proposed in chapter 5 predicts that if the real interfacial thickness is replaced by a larger one, the Peclet number should be increased. For large scale systems, this means that the numerical value of the Peclet number can become very large. In this thesis, we used the Euler explicit method for time integration. However, for large Peclet numbers the local balance equation for the concentration becomes convection dominated and, in this case, the Euler explicit method is stable only for very small time steps. Therefore, to be able to make a proper comparison to classical results, it is advisable to use an operator splitting technique (Timmermans *et al.*, 1994) or another time integration technique, such as a high order Runge-Kutta scheme.

Secondly, moving interfaces can lead to computational difficulties when the interfacial thickness is decreased. To be able to make a comparison with the classical results and to test the scaling is it also necessary to use interfacial thicknesses smaller than those used in chapter 5. The use of a high order spectral element approximation generally allows us to

capture an interface with a small thickness with the same accuracy using less nodal points (Verschueren *et al.*, 1998). However, increasing the order of the element generally increases the required CPU-time. The use of high-order elements can be made more efficient by using finite element pre-conditioning techniques (Anderson, 1999), but even then we can not decrease the interfacial thickness much further because the moving interfaces force us to use a fine mesh everywhere in the domain. In chapter 4, where we considered pinned interfaces, we could easily choose the interfacial thickness as small as one per mille of the computational domain, because we were able to use local mesh refinement near the interface in that case. For moving interfaces, an adaptive re-meshing technique is required if one wishes to have local refinement near the interface at all times.

The results presented in this thesis show that the diffuse-interface approach is a very powerful tool: topological changes are dealt with in a physically justified way and the model, even though it is essentially a small-scale model, can also be applied to large-scale systems. The results, even though preliminary, show that, if the proper scaling is used, the diffuse-interface approach is capable of bridging the gap between small-scale and large-scale systems. Furthermore, the diffuse-interface model can easily be extended to include visco-elastic effects or chemical reactions and the numerical implementation can also be adapted for three dimensional systems.

Appendix A

THERMODYNAMIC RELATIONS

A.1 Gibbs relation: derivation of equations (2.54) and (2.55)

Consider a homogeneous mixture of N fluids. The total internal energy U can be written as

$$U = U(S, V, \{M_i\}) \qquad i = 1 \ldots N , \tag{A.1}$$

where S is the total entropy, V is the total volume, M_i is the total mass of component i and $\{M_i\}$ denotes the set $\{M_1, M_2, \ldots, M_N\}$. The total differential yields the classical Gibbs relation

$$T dS = dU + p dV - \sum_{i=1}^{N} \mu_i d M_i , \tag{A.2}$$

where the temperature T, the pressure p and chemical potential μ_i of component i are given by

$$T = \left(\frac{\partial U}{\partial S} \right)_{V, \{M_i\}} , \qquad p = \left(\frac{\partial U}{\partial V} \right)_{S, \{M_i\}} \qquad \text{and} \quad \mu_i = \left(\frac{\partial U}{\partial M_i} \right)_{S, V, \{M_{j \neq i}\}} , \tag{A.3}$$

respectively. The subscripts denote the constraints, that is, which variables are kept constant. In the rest of this appendix we will omit these subscripts. Dividing the classical Gibbs relation by the total mass M we obtain

$$T ds = du - \frac{p}{\rho^2} d\rho - \sum_{i=1}^{N} \mu_i d c_i , \tag{A.4}$$

where $s = S/M$ is the specific entropy, $u = U/M$ is the specific internal energy, $\rho = M/V$ is the density of the mixture and c_i is the mass fraction of component i.

Now we rewrite the pressure, the temperature and the chemical potentials in terms of the specific internal energy u, which is a function of the specific s entropy and the densities $\{\rho_i\}$: that is

$$u = u(s, \{\rho_i\}) \qquad i = 1 \ldots N . \tag{A.5}$$

Carefully taking into account the constraints used in (A.3), the chemical potential can be rewritten as

$$\mu_i = \frac{\partial \rho u V}{\partial M_i} = V \frac{\partial \rho u}{\partial \rho_i} \frac{\partial \rho_i}{\partial M_i} + V \frac{\partial \rho u}{\partial s} \frac{\partial s}{\partial M_i} = \frac{\partial \rho u}{\partial \rho_i} - \frac{s}{\rho} \frac{\partial \rho u}{\partial s} \tag{A.6}$$

and the temperature as

$$T = \frac{\partial \rho u V}{\partial S} = \frac{\partial \rho u V}{\partial s} \frac{\partial s}{\partial S} = \frac{1}{\rho} \frac{\partial \rho u}{\partial s} = \frac{\partial u}{\partial s} . \tag{A.7}$$

Combining these relations we obtain

$$\mu_i = \frac{\partial \rho u}{\partial \rho_i} - T s . \tag{A.8}$$

The pressure can be rewritten as

$$p = -\sum_{i=1}^{N} \frac{\partial \rho u V}{\partial \rho_i} \frac{\partial \rho_i}{\partial V} = \sum_{i=1}^{N} \frac{\partial \rho u}{\partial \rho_i} \frac{M_i}{V} + \rho u \sum_{i=1}^{N} \frac{\partial V}{\partial \rho_i} \frac{M_i}{V^2} = \sum_{i=1}^{N} \frac{\partial \rho u}{\partial \rho_i} \rho_i - \rho u . \tag{A.9}$$

Combining this relation with (A.8) yields

$$p = \sum_{i=1}^{N} \rho_i \mu_i - \rho u + \rho T s . \tag{A.10}$$

The specific internal energy u is a locally defined variable. The gradient densities can be added as independent variables:

$$u = \hat{u}(s, \{\rho_i\}, \{\nabla \rho_i\}) \qquad i = 1 \dots N . \tag{A.11}$$

The non-classical Gibbs relation now reads

$$T ds = d\hat{u} - \frac{p}{\rho^2} d\rho - \sum_{i=1}^{N} \mu_i dc_i - \sum_{i=1}^{N} \frac{\partial \hat{u}}{\partial \nabla \rho_i} \cdot d\nabla \rho_i . \tag{A.12}$$

Even though the system is no longer homogeneous, we can still use (A.8) and (A.10) as local definitions of the chemical potential and the pressure: that is

$$\mu_i = \frac{\partial \rho \hat{u}}{\partial \rho_i} - T s \tag{A.13}$$

and

$$p = \sum_{i=1}^{N} \rho_i \mu_i - \rho \hat{u} + \rho T s , \tag{A.14}$$

where $\partial \rho \hat{u} / \partial \rho_i$ is now such that also the density gradients $\{\nabla \rho_i\}$ are kept constant. The chemical potential (A.13) and the pressure (A.14) can be identified with μ_{oi} and p_o as defined in equation (2.55).

A.2 Quasi-incompressible systems: derivation of equation (2.76)

The chemical potential (A.13) for component i can be rewritten as

$$\mu_i = \frac{\partial \rho \hat{u}}{\partial \rho_i} - Ts = f + \rho \frac{\partial \hat{u}}{\partial \rho_i} , \qquad (A.15)$$

where $f = \hat{u} - Ts$ is the specific Helmholtz free energy. For quasi-incompressible, isothermal systems the densities depend only on mass fractions $\{c_i\}$. Therefore, we may write

$$\hat{u} = \hat{u}(s, \{c_i\}, \{\nabla c_i\}) \qquad i = 1 \ldots N . \qquad (A.16)$$

Consequently,

$$\frac{\partial \hat{u}}{\partial \rho_i} = \sum_{k=1}^{N} \frac{\partial \hat{u}}{\partial c_k} \frac{\partial c_k}{\partial \rho_i} = \frac{1}{\rho} \sum_{k=1}^{N} \frac{\partial \hat{u}}{\partial c_k} (\delta_{ik} - c_k) , \qquad (A.17)$$

where δ_{ik} is the Kronecker delta. Combining (A.15) and (A.17) we obtain

$$\mu_i = f - \sum_{k=1}^{N-1} c_k \left(\frac{\partial \hat{u}}{\partial c_k} - \frac{\partial \hat{u}}{\partial c_N} \right) + \left(\frac{\partial \hat{u}}{\partial c_i} - \frac{\partial \hat{u}}{\partial c_N} \right) , \qquad (A.18)$$

where we used $\sum_{i=1}^{N} c_i = 1$. Furthermore, combining (A.14) and (A.18), we naturally obtain $p = 0$. Using

$$\hat{u} = u(s, \{c_i\}, \{\nabla c_i\}) \qquad i = 1 \ldots N - 1 , \qquad (A.19)$$

the homogeneous part of the Gibbs relation for quasi-incompressible systems can be written as

$$Tds = du - \sum_{i=1}^{N-1} \frac{\partial u}{\partial c_i} dc_i , \qquad (A.20)$$

where

$$\frac{\partial u}{\partial c_i} = \frac{\partial \hat{u}}{\partial c_i} - \frac{\partial \hat{u}}{\partial c_N} . \qquad (A.21)$$

To obtain the non-classical Gibbs relation we have to rewrite the last term on the right hand side of equation (A.12) in terms of the mass fractions. For quasi-incompressible systems $\partial \hat{u} / \partial \nabla \rho_i$ and $d \nabla \rho_i$ can be rewritten as

$$\frac{\partial \hat{u}}{\partial \nabla \rho_i} = \sum_{k=1}^{N} \frac{\partial \hat{u}}{\partial \nabla c_k} \frac{\partial \nabla c_k}{\partial \nabla \rho_i} \qquad (A.22)$$

and

$$d \nabla \rho_i = \sum_{k=1}^{N} \frac{\partial \nabla \rho_i}{\partial \nabla c_k} d \nabla c_k , \qquad (A.23)$$

respectively. The partial differentials $\partial \nabla c_k / \partial \nabla \rho_i$ and $\partial \nabla \rho_i / \partial \nabla c_k$ can be written as

$$\frac{\partial \nabla c_k}{\partial \nabla \rho_i} = \frac{\partial \nabla (\rho_k / \rho)}{\partial \nabla \rho_i} = \frac{1}{\rho} (\delta_{ik} - c_k) \tag{A.24}$$

and

$$\frac{\partial \nabla \rho_i}{\partial \nabla c_k} = \frac{\partial \nabla (\rho c_i)}{\partial \nabla c_k} = \rho (\delta_{ik} - \rho_i / \varrho_k) , \tag{A.25}$$

respectively, where we used the simple mixture relation: $\rho^{-1} = \sum_{i=1}^{N} c_i / \varrho_i$. Consequently, the non-classical term in the Gibbs relation can be written as

$$\sum_{i=1}^{N} \frac{\partial \hat{u}}{\partial \nabla \rho_i} \cdot d\nabla \rho_i = \sum_{i=1}^{N} \left(\sum_{j=1}^{N} (\delta_{ij} - c_j) \frac{\partial \hat{u}}{\partial \nabla c_j} \right) \cdot \left(\sum_{k=1}^{N} (\delta_{ik} - \rho_i / \varrho_k) d\nabla c_k \right) , \tag{A.26}$$

which yields

$$\sum_{i=1}^{N} \frac{\partial \hat{u}}{\partial \nabla \rho_i} \cdot d\nabla \rho_i = \sum_{i=1}^{N} \frac{\partial \hat{u}}{\partial \nabla c_i} \cdot d\nabla c_i = \sum_{i=1}^{N-1} \frac{\partial u}{\partial \nabla c_i} \cdot d\nabla c_i , \tag{A.27}$$

where

$$\frac{\partial u}{\partial \nabla c_i} = \frac{\partial \hat{u}}{\partial \nabla c_i} - \frac{\partial \hat{u}}{\partial \nabla c_N} . \tag{A.28}$$

Finally, the non-classical Gibbs can be written as

$$T ds = du - \sum_{i=1}^{N-1} \frac{\partial u}{\partial c_i} dc_i - \sum_{i=1}^{N-1} \frac{\partial u}{\partial \nabla c_i} \cdot d\nabla c_i , \tag{A.29}$$

which is indeed identical to equation (2.76).

A.3 Stress tensor: derivation of equation (2.90)

The reversible part of the stress tensor τ_r, given by equation (2.79) reads

$$\tau_r = - \sum_{i=1}^{N-1} \rho \frac{\partial u}{\partial \nabla c_i} \nabla c_i . \tag{A.30}$$

The divergence of τ_r, which appears in the momentum equation, can be written as

$$\nabla \cdot \tau_r = -\rho \sum_{i=1}^{N-1} \frac{\partial u}{\partial \nabla c_i} \cdot \nabla \nabla c_i - \sum_{i=1}^{N-1} \nabla \cdot \left(\rho \frac{\partial u}{\partial \nabla c_i} \right) \nabla c_i . \tag{A.31}$$

Using chemical potential, defined by equation (2.81), we obtain

$$\nabla \cdot \tau_r = -\rho \sum_{i=1}^{N-1} \frac{\partial u}{\partial \nabla c_i} \cdot \nabla \nabla c_i + \rho \sum_{i=1}^{N-1} (\mu_i - \mu_N) \nabla c_i - \rho \sum_{i=1}^{N-1} \frac{\partial u}{\partial c_i} \nabla c_i . \tag{A.32}$$

The gradient of u can be written as

$$\nabla u = \frac{\partial u}{\partial s}\nabla s + \sum_{i=1}^{N-1} \frac{\partial u}{\partial c_i}\nabla c_i + \sum_{i=1}^{N-1} \frac{\partial u}{\partial \nabla c_i}\cdot\nabla\nabla c_i .$$

(A.33)

Combining (A.32), (A.33) and (A.7) we obtain

$$\nabla\cdot\tau_r = -\rho\nabla u + \rho T\nabla s + \rho\sum_{i=1}^{N-1}(\mu_i - \mu_N)\nabla c_i .$$

(A.34)

For isothermal systems, this can be written as

$$\nabla\cdot\tau_r = -\rho\nabla f + \rho\sum_{i=1}^{N-1}(\mu_i - \mu_N)\nabla c_i ,$$

(A.35)

which is identical to equation (2.90).

BIBLIOGRAPHY

Anderson, D. M., McFadden, G. B., and Wheeler, A. A. (1998). Diffuse-interface methods in fluid mechanics. *Annu. Rev. Fluid Mech.*, **30**, 139–165.

Anderson, P. D. (1999). *Computational analysis of distributive mixing*. Ph.D. thesis, Eindhoven University of Technology, the Netherlands.

Antanovskii, L. K. (1995). A phase-field model of capillarity. *Phys. Fluids*, **7**, 747–753.

Barton, B. F., Graham, P. D., and McHugh, A. J. (1998). *Macromolecules*, **31**, 1672.

Bates, P. W. and Fife, P. C. (1993). The dynamics of nucleation for the Cahn-Hilliard equation. *SIAM J. Appl. Math.*, **53**(4), 990–1008.

Bazhlekov, I. B., Chesters, A. K., and van de Vosse, F. N. (1999). The effect of the dispersed to continuous-phase viscosity ratio on film drainage between interacting drops. *Int. J. Multiphase Flow.* (in press).

Bearman, R. J. and Kirkwood, J. G. (1958). Statistical mechanics of transport processes. XI. Equations of transport in multicomponent systems. *J. Chem. Phys.*, **28**(1), 136–145.

Bensimon, D., Kadanoff, L. P., Liang, S., Shraiman, B. I., and Tang, C. (1986). Viscous flows in two dimensions. *Rev. Mod. Phys.*, **58**(4), 977–999.

Berghmans, S. (1995). *Spinning of hollow fibres*. Ph.D. thesis, Leuven, Belgium.

Bird, R. B., Stewart, W. E., and Lightfoot, E. N. (1960). *Transport Phenomena*. Wiley.

Blinowski, A. (1975). Gradient description of capillary phenomena in multicomponent fluids. *Arch. Mech.*, **27**(2), 273–292.

Boos, W. and Thess, A. (1997). Thermocapillary flow in a Hele-Shaw cell. *J. Fluid Mech.*, **352**, 305–330.

Brackbill, J. U., Kothe, D. B., and Zemach, C. (1991). A continuum model for modeling surface tension. *J. of Comp. Phys.*, **100**, 335–354.

Cahn, J. W. (1964). Phase separation by spinodal decomposition in isotropic systems. *J. Chem. Phys.*, **42**(1), 93–99.

Cahn, John W. and Hilliard, John E. (1958). Free energy of a nonuniform system. I. Interfacial energy. *J. Chem. Phys.*, **28**(2), 258–267.

Cahn, John W. and Hilliard, John E. (1959). Free energy of a nonuniform system. III. *J. Chem. Phys.*, **31**, 688–699.

Chesters, A. K. (1991). The modelling of coalescence in fluid-liquid dispersions: a review of current understanding. *Trans. Inst. Chem. Engrs. Part A*, **69**, 259–270.

Davis, H. T. and Scriven, L. E. (1982). Stress and structure in fluid interfaces. *Adv. Chem. Phys.*, **49**, 357–454.

Davis, S. H. (1987). Thermocapillary instabilities. *Ann. Rev. Fluid Mech.*, **19**, 403–435.

Debye, P. (1959). *J. Chem. Phys.*, **31**, 680.

Dell'Isola, F., Gouin, H., and Rotoli, G. (1996). Nucleation of spherical shell-like interfaces by secon gradient theory: numerical simulations. *Eur. J. Mech. B/Fluids*, **15**(4), 545–568.

Doi, M. (1996). *Introduction to polymer physics*. Clarendon Press, Oxford.

Dussan V, E. B. and Davis, S. H. (1974). On the motion of a fluid-fluid interface along a surface. *J. Fluid Mech.*, **65**, 71–95.

Edwards, D. A., Brenner, H., and Wassan, D. T. (1991). *Interfacial transport processes and rheology*. Butterworth Heinemann.

Elliot, C. M. (1989). The Cahn-Hilliard model for the kinetics of phase separation. *Int. Ser. Num. Math.*, **88**, 35.

Evans, R. (1979). *Adv. Phys.*, **28**, 143.

Gunton, J. D., Miguel, M. S., and Sahni, P. S. (1983). *The dynamics of first-order phase transitions*, volume 8 of *Phase transitions and critical phenomena*. Academic Press, London.

Gurtin, M. E., Polignone, D., and Viñals, J. (1996). Two-phase binary fluids and immiscible fluids described by an order parameter. *Math. Models Methods Appl. Sci.*, **6**, 815.

Helfand, E. (1982). *Polymer compatibility and incompatibility: principles and practice*, volume 2 of *MMI Symp. Ser.*

Helfand, E. and Sapse, A. M. (1976). Theory of the concentrated polymer solution/solvent interface. *J. Polymer Sci.*, **54**, 289–297.

Helfand, E. and Tagami, Y. (1972). Theory of the interface between immiscible polymers. II. *J. Chem. Phys.*, **56**, 3592.

Hohenberg, P. C. and Halperin, B. I. (1977). Theory of dynamical critical phenomena. *Rev. Mod. Phys.*, **49**, 435.

Hyman, J. M. (1984). Numerical methods for tracking interfaces. *Physica D*, **12**, 396–407.

Jacqmin, D. (1996). An energy approach to the continuum surface tension method. In *Proc. 34th Aerosp. Sci. Meet. Exh. AIAA 96-0858*, Reno. Am. Inst. Aeron. Astron.

Jasnow, D. and Viñals, J. (1996). Coarse-grained description of thermo-capillary flow. *Phys. Fluids*, **8**(3), 660–669.

Joseph, D D. and Renardy, Y Y. (1993). *Fundamentals of two-fluid dynamics*. Springer-Verslag, New York.

Kikuchi, R. and Cahn, J. W. (1962). Theory of domain walls in ordered structures II. Pair approximation for nonzero temperatures. *J. Phys. Chem. Solids*, **23**, 137–151.

Kuhlmann, Hendrik C. (1999). *Thermocapillary convection in models of crystal growth*. Springer, Berlin.

Landau, L. D. and Lifshitz, E. M. (1959). *Fluid Mechanics*. Pergamon, New York.

Lifschitz, M. and Freed, K. F. (1993). Interfacial behavior of compressible polymer blends. *J. Chem. Phys.*, **98**(11), 8994–9013.

Lowengrub, J. and Truskinovsky, L. (1998). Quasi-incompressible Cahn Hilliard fluids. *Proc. R. Soc. London Ser. A*, **454**, 2617–2654.

Lowengrub, J., Goodman, J., Lee, H., Longmire, E.K., Shelley, M. J., and Truskinovsky, L. (1998). Topological transitions in liquid/liquid interfaces. In I. Athanasopoulos, M. Makrakis, and J. F. Rodrigues, editors, *Proceedings of the 1997 International Congress on Free Boundary Problems*, Pitman Research Notes. Addison-Wesley Longman.

Manickam, O. and Homsy, G. M. (1995). Fingering instabilities in vertical miscible displacement flows in porous media. *J. Fluid Mech.*, **288**, 75–102.

McMullen, W. E. (1991). Nonlocal contributions to the thermodynamics of inhomogeneous homopolymer-solvent systems. *J. Chem. Phys.*, **95**(11), 8507–8520.

Patera, A. T. (1984). A spectral element method for fluid dynamics. *J. Comp. Phys.*, **54**, 468–488.

Pego, R. L. (1989). Front migration in the nonlinear Cahn-Hilliard equation. *Proc. Roy. Soc. Lond. A*, **422**, 261–278.

Prigogine, I. (1961). *Introduction to thermodynamics of irreversible processes*. Interscience, London.

Rother, M. A., Zinchenko, A. Z., and Davis, R. H. (1997). *F. Fluid Mech.*, **346**, 117–148.

Rowlinson, J. S. and Widom, B. (1989). *Molecular Theory of Capillarity*. Oxford, Clarendon.

Saffman, P. G. and Taylor, G. I. (1958). *Proc. R. Soc. London, Ser. A*, **245**, 312.

Seppecher, P. (1996). Moving contact lines in the Cahn-Hilliard theory. *Int. J. Eng. Sci.*, **34**(9), 977–992.

Sherwood, Thomas K. and Wei, James C. (1957). Interfacial phenomena in liquid extraction. *Ind. Eng. Chem.*, **49**, 1030–1034.

Sternling, C V. and Scriven, L E. (1959). Interfacial turbulence: hydrodynamic instability and the Marangoni effect. *AIChE J.*, **5**, 514–523.

Timmermans, L J. P., van de Vosse, F N., and Minev, P D. (1994). Taylor-Galerkin-based spectral element methods for convection-diffusion problems. *Int. J. for Num. Meth. in Fluids*, **18**, 853–870.

Unverdi, S O. and Tryggvason, G. (1992). Computations of multi-fluid flow. *J. Comp. Phys.*, **60**, 70–83.

Verschueren, M., van de Vosse, F.N., and Meijer, H.E.H. (1998). A high order interface capturing technique for structure development in binary fluids. June 22-26, Herzliya, Israel. ICOSAHOM'98.

de Gennes, P. G. (1977). *Scaling concepts in polymer physics*. Cornell university, Ithaca, New York.

de Gennnes, P. G. (1980). Dynamics of fluctuations and spinodal decomposition in polymer blends. *J. Chem. Phys.*, **72**, 4757–4762.

de Groot, S. R. and Mazur, P. (1984). *Non-equilibrium thermodynamics*. Dover Publications, Inc., New York.

van der Waals, J D. (1979). The thermodynamic theory of capillarity under the hypothesis of a continuous density variation. *J. Stat. Phys.*, **20**, 197–244. translated by J.S. Rowlinson.

SUMMARY

Processes such as phase separation, phase inversion, interfacial deformations, coalescence or break-up are frequently encountered in modern technology and industrial processing. Very often, these processes, which can occur simultaneously, are subject to an imposed flow, which ensures that the desired structure is obtained. A better understanding of this way of manipulating structure development can lead to an increase in the quality of industrial products. One way to obtain a better understanding is through modelling.

Several aspects of structure development complicate the development of a suitable physical model and an appropriate numerical implementation. Firstly, modelling of structure development in flow involves both multi-component hydrodynamics and non-equilibrium thermodynamics, which have to be included in a coupled way. Secondly, processes such as phase separation and coalescence involve changes in the interfacial topology: that is, interfaces can intersect or (dis)appear. Thirdly, the length scales involved with structure development range from the macroscopic size of the system to the microscopic molecular interaction length: the flow is normally controlled on a macroscopic level, but the topological changes are controlled by the range of molecular interactions. Bridging this gap between microscopic and macroscopic scales is clearly the biggest challenge in modelling structure development in flow.

The model proposed in this thesis is a diffuse-interface model, which goes back to the ideas of van der Waals. In contrast with the classical sharp-interface model, an interface between immiscible fluids is represented by a continuous concentration profile. The thickness of the interface is closely related to the range of molecular interactions. Thermodynamically, the finite interaction range is represented by a non-local effect in the free energy: the local free energy density not only depends on the local composition, but also on the composition of the immediate environment. Cahn and Hilliard used a Taylor expansion of the free energy density about the homogeneous state. In this way, the non-local effect is represented by a dependence on local composition gradients rather than non-local composition. Including the non-local effect in this way, non-classical expressions for the chemical potential, the stress tensor and the energy flux are derived in this thesis, following the principles of classical irreversible thermodynamics. The obtained expressions have a differential form, which allows a direct coupling with the equations of fluid dynamics.

The obtained set of non-classical governing equations combines multi-component hydrodynamics and non-equilibrium thermodynamics. Furthermore, changes in interfacial topology are included in a physically justified way, since the molecular interaction length which controls the topological changes is included in the model. Computationally, the diffuse-interface approach also has some advantages over the classical sharp-interface approach, in which boundary conditions are applied to connect the bulk phases. The non-classical expression for the stress tensor includes interfacial tension as a body force in the momentum equation, which makes a direct application of boundary conditions not necessary. This means that a fixed grid numerical technique can be used, which is convenient in case the topology of the interface changes.

In this thesis the diffuse-interface model is applied to several phenomena: phase separation, interfacial instabilities, thermo-capillary flow and coalescence. For the initial stages of phase separation the interfacial thickness, which is typically of the order 0.1 nm, can be cap-

tured numerically and the model can be directly applied. For large-scale systems, in which the real interfacial thickness can not be captured numerically, scaling needs special attention. In this thesis it is argued that, if the interface is replaced by one with a numerically acceptable thickness, scaling should be such that interfacial tension retains its value. Using this scaling, it is shown that the diffuse-interface results for thermo-capillary flow converge to the classical results for pinned interfaces. In case of moving interfaces and topological changes, an additional scaling of the diffusion term is required. Applying the same scaling which is used for the capillary term to diffusion it is found that the diffusional Peclet number is proportional to the dimensionless interfacial thickness. This scaling is different from the ones used in literature, which are based on obtaining the classical equations in the sharp-interface limit. Results for coalescence of fluid domains in hyperbolic flows indicate that the scaling proposed in this thesis performs better than the scaling used in literature: when the interfacial thickness is replaced by a larger one, the obtained spread in coalescence times for the scaling proposed in this thesis is typically about four times smaller than for the other scaling.

SAMENVATTING

Structuurontwikkeling is een essentieel onderdeel van veel moderne industriële processen en technologieën. Processen als fasenscheiding, faseninversie, deformaties van het scheidingsvlak tussen vloeistoffen en het samenvloeien of opbreken van vloeistofdomeinen kunnen de structuur(ontwikkeling) beïnvloeden. Eigenschappen van producten worden bepaald door de structuur. Voorbeelden zijn de smaak van voedsel, de belastbaarheid van vezels en de kwaliteit van producten als verf, papier en cosmetica. Ook voor technologieën als inkt-jet printen en oliewinning is structuurontwikkeling van belang. Om de gewenste structuur te krijgen is het vermogen om de structuurontwikkeling tijdens het proces te sturen en manipuleren essentieel. Soms wordt een extern opgelegd snelheidsveld gebruikt om de structuur te beïnvloeden. Een bekend alledaags voorbeeld hiervan is het kloppen van slagroom.

Fysische modellering is een manier om een beter inzicht te krijgen in de processen die een rol spelen tijdens structuurontwikkeling. Het modelleren van structuurontwikkeling is moeilijk om een aantal redenen. Ten eerste kunnen meerfasenstroming en niet-evenwichts thermodynamica niet ontkoppeld worden: structuurontwikkeling door fasenscheiding kan in principe beïnvloed worden door een opgelegde stroming. Verder moet er bij de numerieke implementatie van het model rekening mee gehouden worden dat er veranderingen in de topologie van de scheidingsvlakken tussen de vloeistoffen kunnen optreden. Ten derde spelen lengteschalen een rol die variëren van de macroscopische afmetingen van het systeem tot de schaal van microscopische interacties tussen moleculen.

Op het oog lijkt het scheidingsvlak tussen twee niet mengbare vloeistoffen een scherpe overgang. In de klassieke modellering van meerfasenstroming wordt dan ook aangenomen dat er een discontinue overgang is in de concentratie. Eigenschappen als oppervlaktespanning worden opgelegd via randvoorwaarden. Numerieke implementaties van het klassieke model maken vaak gebruik van een discretisatie waarbij de knooppunten het scheidingsvlak volgen, zodat de randvoorwaarden op een eenvoudige manier kunnen worden opgelegd. Deze vorm van discretisatie leidt tot moeilijkheden als er topologisch veranderingen in het scheidingsvlak tussen de vloeistoffen optreedt. Deze tekortkoming heeft ook een fysische achtergrond: topologische veranderingen worden veroorzaakt door moleculaire interacties in de buurt van het scheidingsvlak. De moleculaire interactielengte, die niet in de klassieke modellering wordt meegenomen, is daarom een belangrijke parameter.

Het model in dit proefschrift is een zogenaamd 'diffuse-interface' model (diffuus-scheidingsvlak model). De basis voor dit model is gelegd door Van der Waals. De essentie van het model is dat een scheidingsvlak tussen twee niet mengbare vloeistoffen diffuus verondersteld wordt. Met andere woorden, er wordt aangenomen dat het verloop in de concentratie van de ene naar de andere vloeistof continu is. De afstand waarover de concentratie varieert wordt bepaald door de moleculaire interactielengte die nauw samenhangt met de dikte van het scheidingsvlak. Thermodynamisch gezien komt deze interactielengte tot uiting in een niet-locaal effect in de vrije-energiedichtheid van het systeem: de vrije-energiedichtheid hangt niet alleen af van de locale waarde van de concentratie, maar ook van de waarden van de concentratie in de nabije omgeving. Gebruik makend van een Taylor-ontwikkeling van de vrije-energiedichtheid om de homogene toestand, kan het niet-locale effect worden vertaald naar een afhankelijkheid van locale concentratiegradiënten. Uitgaande van deze representatie

van het niet-locale effect, worden in dit proefschrift niet-klassieke uitdrukkingen voor de chemische potentiaal, de spanningstensor en de energieflux afgeleid. Deze uitdrukkingen hebben een differentiaalvorm, waardoor ze eenvoudig te koppelen zijn met de locale behoudswetten voor massa, impuls en energie. De op deze manier verkregen set vergelijkingen stelt ons in staat om structuurontwikkeling tijdens stroming te simuleren. Het model omvat zowel meerfasenstroming als niet-evenwichtsthermodynamica. Verder zorgt de continue representatie van het scheidingsvlak ervoor dat oppervlaktespanning als een volumekracht wordt meegenomen in de impulsvergelijking. Hierdoor is het opleggen van randvoorwaarden niet meer nodig.

In dit proefschrift wordt het 'diffuse-interface' model toegepast op fasenscheiding, instabiliteiten in scheidingvlakken tussen vloeistoffen, thermocapillaire stroming en samenvloeiing van vloeistofdomeinen. Voor de meeste systemen is de dikte van het scheidingsvlak erg klein: een typische waarde is 0.1 nanometer. Dit betekent dat het 'diffuse-interface' model alleen direct kan worden toegepast op kleinschalige systemen, zoals bijvoorbeeld de initiatie van fasenscheidingsprocessen. Voor processen die plaatsvinden op een grotere schaal is het meestal niet mogelijk om de echte waarde van de dikte van het scheidingsvlak te gebruiken. Het is dan noodzakelijk om het echte scheidingsvlak te vervangen door een scheidingsvlak met een numeriek acceptabele dikte. In dat geval moet er extra aandacht besteed worden aan de schaling: de schaling moet dusdanig zijn dat het systeem met het dikkere scheidingsvlak zich hetzelfde gedraagt als het originele systeem. De in dit proefschrift voorgestelde schaling zorgt ervoor dat de oppervlaktespanning niet verandert als de dikte van het scheidingsvlak verandert. De resultaten voor thermocapillaire stroming in dit proefschrift tonen aan dat, voor systemen waarbij geen topologieveranderingen optreden, het scheidingsvlak inderdaad mag worden vervangen door een andere: de resultaten convergeren naar de klassieke oplossing als de scheidingsvlakdikte naar nul gaat. Voor systemen waarin wel topologieveranderingen optreden, zoals samenvloeiing van vloeistofdomeinen, levert de in dit proefschrift voorgestelde schaling een kleinere spreiding in de resultaten bij verandering van de scheidingsvlakdikte dan een schaling die gebruikelijk is in de literatuur.

DANKWOORD

CURRICULUM VITAE

24 - 5 -1971:   geboren te Nieuw-Ginneken

1983-1989:   VWO, Mencia de Mendoza Lyceum, Breda

1989-1995:   Technische Natuurkunde, TU Eindhoven

1995-1999:   AIO-4, Materials Technology, TU Eindhoven

Stellingen

behorende bij het proefschrift

A Diffuse-Interface Model for Structure Development in Flow

1. De moleculaire interactielengte speelt een belangrijke rol tijdens structuurontwikkeling en mag daarom niet zonder meer worden weggelaten uit de modellering.
   - Dit proefschrift.

2. Zowel vanuit fysisch als numeriek oogpunt verdient het 'diffuse-interface' model de voorkeur boven de klassieke modellering.
   - Dit proefschrift.

3. Indien er geen veranderingen in de topologie van een scheidingsvlak tussen niet-mengbare vloeistoffen optreden mag de scheidingsvlakdikte vervangen worden door een grotere, mits de juiste schaling wordt toegepast.
   - Dit proefschrift, Hoofdstuk 4.

4. In de literatuur worden regelmatig incorrecte uitdrukkingen voor de oppervlaktespanning afgeleid. Deze fouten worden niet opgemerkt als er geen vergelijking met experimenten of met resultaten van andere modellen plaatsvindt.
   - Jasnow, D. and Viñals J. (1996). Coarse-grained description of thermocapillary flow. *Phys. Fluids*, **8**(3), 660-669
   - Gurtin, M.E., Polignone D., Viñals J. (1996). Two-phase binary fluids and immiscible fluids described by an order parameter. *Math. Models Methods Appl. Sci.*, **6**, 815-831.

5. De wetenschap- en techniekvoorlichting is in Nederland gefundeerd op een democratische en een economische pijler. De democratische pijler dreigt nu uit het zicht te verdwijnen.
   - Rapport over de instelling van een dienst wetenschapsvoorlichting, KNAW, mei 1977.
   - N. Wiedenhof,*Aarde, Appel, Ei, wetenschaps- en techniekvoorlichting in Nederland en ook wat daarbuiten 1985-1995*, rapport aan de stichting PWT, Stichting Publiek, Wetenschap, Techniek (inmiddels opgegaan in WeTeN), Utrecht 1995.
   - Kiezen voor Kracht en Kwaliteit, rapport evaluatie van de stichting WeTeN i.o.v. ministeries van OCenW en EZ, Den Haag, mei 1999. Zie ook Persbericht OCenW, Conclusies evaluatie Stichting WeTeN, 16 juni 1999.

6. Bureaucratie wordt meestal voelbaar door een onvolledige of ondoorzichtige voorlichting naar het publiek toe over de te volgen procedures.

7. Vanuit het oogpunt van de lezer is Japans een efficiënte taal.

8. Voor veel wetenschappelijk onderzoek is serendipiteit essentieel.

9. Het belang van het visuele aspect van een muzikaal optreden is ouder dan de videoclip.

10. Lange sommen zijn vervelend.

Maykel Verschueren,
Eindhoven, 4 oktober 1999.